LASER
& PHOTONICS
REVIEWS

Laser Photonics Rev. **9,** No. 3, 275–293 (2015) / **DOI** 10.1002/lpor.201400208

Abstract Recent studies have demonstrated that femtosecond laser pulses have high potential in application to environmental science. Because of the properties of *ultrafast*, *broadband* and *high power*, the propagation of femtosecond laser pulses in air can lead to the generation of a strong field of 10^{13}–10^{14} W/cm^2 with a large distance range from meter to kilometers. The strong laser field induces ionization and fragmentation of molecules in the laser propagation path, resulting in characteristic fingerprint emissions. This paper mainly focuses on recent research advances in environmental sensing by using femtosecond laser pulses through strong-field-induced ionization and fragmentation of molecules. The fingerprint emissions of molecules in strong laser fields are discussed based on the understanding of strong-field–molecule interactions in atmospheric as well as in vacuum environments. This is followed by a comprehensive review of several recently developed optical methods for coherent control of fingerprint emissions of molecules. Lastly, both current challenges and a future perspective of this dynamic field are discussed.

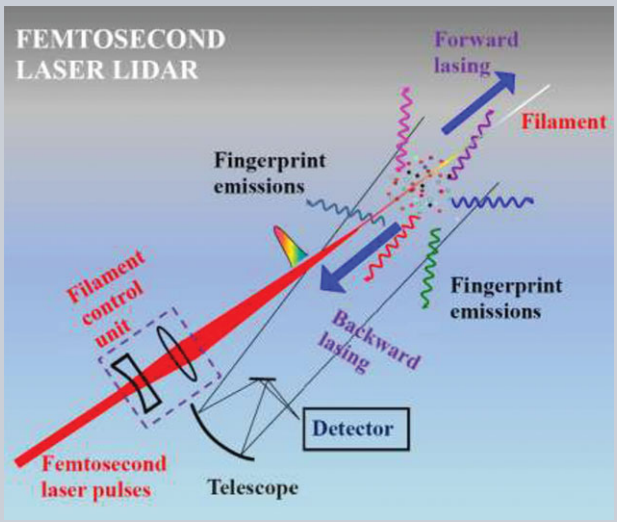

REVIEW
ARTICLE

Femtosecond laser ionization and fragmentation of molecules for environmental sensing

Huailiang Xu[1], Ya Cheng[2,*], See-Leang Chin[3], and Hong-Bo Sun[1,4,*]

1. Introduction

Innovative progress of ultrafast laser technologies in the last three decades has enabled scientists to generate strong laser fields whose electric field strength is comparable to or even exceeds that of the Coulomb-binding field within molecules [1]. In the presence of such strong laser fields, molecules exhibit many intriguing behaviors such as high-order harmonic generation [2], bond softening and hardening [3], and rotational excitation and molecular alignment [4]. Thanks to these spectacular findings, strong-field molecular physics has become an important subject of contemporary physics and has already triggered a broad range of applications including molecular orbital imaging [5], coherent X-ray sources [6], material processing [7, 8], femtosecond and attosecond chemistry [9], and so forth. Still, after nearly two decades of intensive investigations, new phenomena and new effects emerge in this field, among which a unique nonlinear optical phenomenon called "femtosecond laser filamentation" resulting from the propagation of femtosecond laser pulses in transparent optical media has attracted much attention in these years [10–15]. This nonlinear phenomenon can give rise to a high nearly constant laser intensity of about 10^{13}–10^{14} W/cm^2 [16, 17] in a large distance range from meters to kilometers in the atmosphere, opening up the possibility of investigating strong-field molecule interaction at a remote place in a variety of complicated environments such as atmosphere and combustion flames [18, 19].

Due to a variety of nonlinear effects of atoms/molecules induced by such strong fields in a filament [20–22], the subject of femtosecond laser filamentation has been a hot research topic, associating with a lot of potentially challenging physics and applications such as THz radiation generation [23–27], lightning and weather control [28–32], remote air lasing [33–37], few-cycle pulse generation [38, 39], and high-harmonic generation [40–42]. In particular, the laser intensity inside a filament is high enough to induce remote ionization and fragmentation of molecules [16, 17, 43–45], giving rise to characteristic fingerprint fluorescence emissions from the ionized molecules or fragments that could be used for identifying the parent molecules. Therefore, it was proposed that filament-induced nonlinear spectroscopy (FINS) through femtosecond laser ionization and fragmentation of molecules could be employed for sensing trace chemical and biological agents and pollutants in the atmosphere [46–48]. It should also be pointed out that an alternative remote atmospheric sensing scheme using

[1] State Key Laboratory on Integrated Optoelectronics, College of Electronic Science and Engineering, Jilin University, Changchun 130012, China
[2] State Key Laboratory of High Field Laser Physics, Shanghai Institute of Optics and Fine Mechanics, Chinese Academy of Sciences, Shanghai, 201800, China
[3] Center for Optics, Photonics and Laser (COPL), Laval University, Quebec City, Quebec G1V 0A6, Canada
[4] College of Physics, Jilin University, Changchun 130012, China
*Corresponding authors: e-mails: ya.cheng@siom.ac.cn, hbsun@jlu.edu.cn

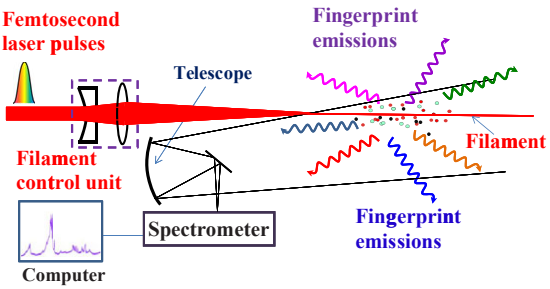

Figure 1 Schematic diagram of femtosecond laser pulses for sensing through the interaction of strong laser field with molecules.

femtosecond laser filaments was proposed in the early 2000s by the Teramobile team in Europe [49], which is based on the ultrabroad spectral content of the self-transformed white-light pulses to provide light source for absorption Lidar [13, 49]. In this review we will only focus our attention on the sensing scheme of FINS associated with femtosecond laser ionization and fragmentation of molecules.

The sensing scheme (see Fig. 1) of FINS possesses several unique properties. First, intense femtosecond laser pulses can project the high intensity through filamentation over a long distance in adverse atmospheric environments with higher robustness against perturbation as compared to weak light propagation [50–53], making FINS a promising technique for remote detection. Secondly, FINS shows a high potential for multicomponents monitoring with only one laser source because strong femtosecond laser field in the filament can simultaneously induce ionization/dissociation of all kinds of gas molecules in the interaction zone, resulting in characteristic fingerprint emissions from excited fragments, atoms or ions [19, 44, 48]. Thirdly, self-induced amplification of fluorescence via amplified spontaneous emission (ASE) or seed amplification could be triggered in filaments to overcome the quenching effect and provides a way to improve the signal-to-noise ratio of FINS [33–37, 54, 55]. These properties of FINS associated with femtosecond laser ionization of molecules would provide several unique advantages for remote sensing when compared with conventional laser-based techniques such as tunable diode laser absorption spectroscopy, polarization spectroscopy and nanosecond laser-induced fluorescence (ns-LIF), all of which have been successfully employed for sensing atmospheric trace species and aerosols with high sensitivities [56–58]. For example, the latter conventional laser sensing techniques usually require coherent laser sources with a particular wavelength for sensing a specific species. This means that the laser may only be optimized for one pollutant at a time.

Despite the high potential of femtosecond laser ionization and fragmentation of molecules in view of applications in environmental sensing, the underlying mechanisms behind the fingerprint emissions of molecules in ambient air are quite complicated, which leave a lot of challenges ahead. On the one hand, when molecules are exposed to such high intensity of 10^{13}–10^{14} W/cm^2, ionization and fragmentation (dissociation) of molecules occur rapidly with the time scale comparable to the laser pulse duration, resulting in fluorescing ions or fragments directly [43, 59–61]. Ideally speaking, ultrafast ionization and fragmentation dynamic of molecules in intense laser fields could be best investigated in a collision-less, hence, vacuum condition by probing electron, ion and photon signals simultaneously. Using the coincidence momentum imaging (CMI) method [62] to visualize the motion of ions (proton) in the interaction process is an important step towards such an ideal measurement. On the other hand, in air (collisional environment), the resultant ions/fragments could interact with the surrounding particles such as electrons, ions and neutral nitrogen/oxygen molecules in a relatively slow time scale, leading to characteristic optical emissions in some cases [43, 63]. Therefore, in terms of the complexity of the FINS spectra, it requires the investigation of strong-laser-field-–molecule interaction in atmospheric as well as in vacuum environments to provide the full physical picture of the fingerprint emissions of molecules in strong laser fields.

The aim of this article is to introduce, discuss and review the main aspects of femtosecond laser ionization and fragmentation of molecules for environmental sensing application. We will give a brief introduction to the physics of femtosecond laser filamentation and present its unique properties for environmental sensing in Section 2. In Section 3 we will demonstrate current research status of this field with a special emphasis on the underlying mechanisms responsible for characteristic emissions of molecules in intense laser fields based on the understanding of strong-field–molecule interaction in atmospheric as well as in vacuum conditions. Several examples of sensing by using femtosecond laser ionization of molecules in atmospheric and combustion environments are given. In Section 4, we will introduce self-generated lasing actions in air induced by strong laser field, which shows the ability to overcome the quenching effect and significantly improve the signal-to-noise ratio in atmospheric and combustion conditions. Lastly, both current challenges and a future perspective of this dynamic field are discussed in Section 5.

2. Propagation of femtosecond laser pulses in the atmosphere

When powerful femtosecond laser pulses propagate in transparent optical media, filamentation occurs as a universal process in all optical media, in which the only difference may be the different generation mechanisms of free electrons in different phase samples of gas, liquid and solid [10–12]. Here we will focus on the discussion of femtosecond laser pulse propagation in gaseous targets, which can result in a constant high field over a long distance inducing remote strong-field−molecule interaction.

2.1. Femtosecond laser filamentation

The physics of femtosecond laser filamentation is now basically understood and a few excellent reviews are already available, to which the readers are suggested to refer to [10–15]. Briefly, femtosecond laser filamentation appears as a result of the dynamic balance between Kerr self-focusing and self-generated plasma defocusing from multiphoton/tunnel ionization of air molecules. This equilibrium leaves a long weak plasma channel (called a filament) behind the laser pulses and clamps the laser intensity inside the filament core to a constant value of about 5×10^{13} W/cm^2 (intensity clamping) with Ti:sapphire laser pulses at 800 nm in air [16,17,64]. This clamped intensity can change slightly, depending on the experimental conditions such as gaseous species [65,66], external focusing conditions [67], and laser polarization and wavelength [22,68]. The resultant plasma density is $\sim10^{14}$–10^{17} cm^{-3} in air [67,69–71]) with a diameter of $\sim$100–200 μm (in air) and a length from a few centimeters up to hundreds of meters, giving rise to the perception of a filament [14]. It should be pointed out that outside the filament core there exists a weak intensity zone called an "energy reservoir", which would not induce any measurable ionization fluorescence signal [14].

During the propagation of a filament in air, processes such as scattering and ionization of molecules would decrease the laser energy, and once the lost energy is large enough to make the peak power of the pulse lower than the "so-called" critical power for self-focusing the filamentation terminates inevitably. In air, the critical power was about 5−10 GW [72,73]. The critical power in air could gradually decrease when the pulse is lengthened through chirping both negatively and positively [73]. Moreover, in some cases the filamentation can be terminated even if the peak power of the pulse is still higher than the critical power, which may result from additional diffraction/divergence of the laser pulses by external optical control during the filamentation process [74].

2.2. Remote control of high intensity filamentation

Femtosecond filamentation could occur over a long distance in the atmosphere, but this requires optimizing the laser parameters such as the pulse chirp and beam diameter. By chirping the pulse negatively to compensate for the group-velocity dispersion (GVD) in air, kilometer-range nonlinear propagation of femtosecond laser pulses was observed [51,75]. Figure 2 shows a typical image of the propagation of a femtosecond TW laser beam in the atmosphere with the parameters of initially 3-cm parallel beam, 150-fs pulse duration and 800-nm wavelength [51]. However, in such a case, multiple filaments of terawatt laser pulses are inevitably generated and compete with each other. The formation of multiple filaments copropagating in air was suggested to come from the inhomogeneous intensity distribution in the transverse cross section of the laser

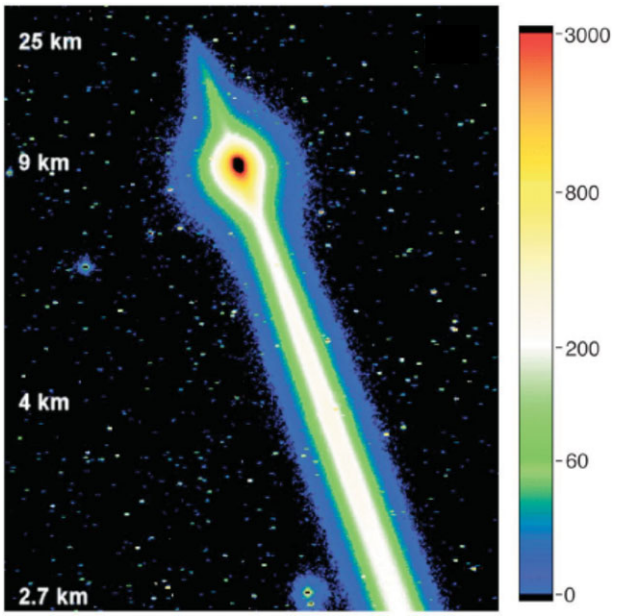

Figure 2 Image taken with a CCD camera of the Tautenburg observatory for kilometer-range nonlinear propagation of femtosecond laser pulses. The horizontal strips across the pictures are stars passing through the telescope field of view. Note the strongly nonlinear altitude scale due to triangulation (with permission of Ref. [51]. Copyright 2004 American Physical Society).

pulse due to either initial laser imperfections arising from the laser source itself or during the propagation through any nonhomogeneous optical medium [76–79]. The competition of multiple filaments gives rise to a random distribution of multiple filaments on the transverse pattern along the propagation path as well as fluctuations of ionization signals on a shot-to-shot basis despite the rather stable laser pulse energy [78]. Many approaches have been proposed so far to control the filamentation by introducing elements such as telescope optics [80,81], phase plates [79,82,83] and apertures [84,85] in order to modify the laser parameters including beam diameter, pulse chirp and input energy, in which the onset position and length of the filaments could be monitored by observing the fluorescence signals of air molecules [86−89]. Other techniques for filamentation control include molecular alignment [90], photonic lattices [91], thermal waveguides [92] and ring-Airy beams [93], etc.

By tilting a focusing lens to introduce beam astigmatism, it was found that multiple filaments could be changed to a single filament [87], but with this method it is difficult to predict the tilting angle of the lens to optimize the formation of the single filament that is strongly dependent on the input power and beam profile. The effect of the laser-beam diameter on the filament formation was also examined [85,88]. By inserting an iris in the propagation path of an initially unfocused pulse, multiple filaments could be controlled. The optimal diameter of the aperture corresponds to the situation where multiple filaments concentrate around the propagation axis to interfere and form a

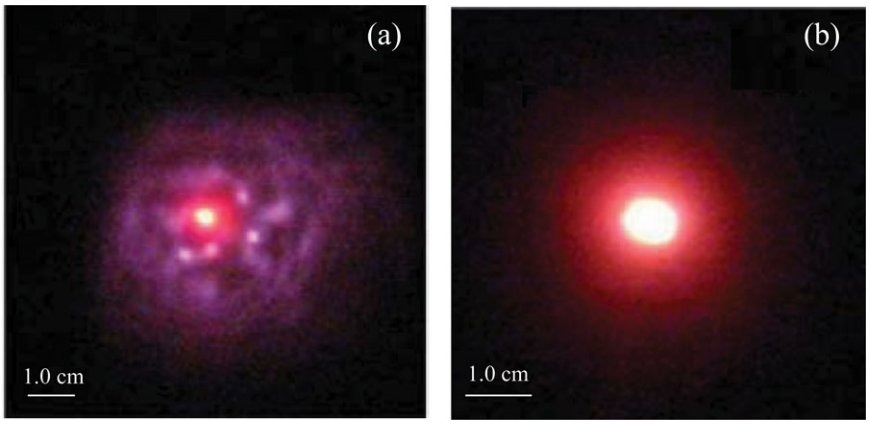

Figure 3 Filament pictures taken with (a) the large beam diameter in the absence of a telescope and (b) the small diameter in the present of an inverted telescope (with permission of Ref. [88]. Copyright 2004 Springer-Verlag).

regularized and elongated structure with a higher overall amount of plasma [85]. On the other hand, when the initial beam diameter of the collimated femtosecond laser pulse was decreased by a telescope from 25 mm to 8 mm with constant input laser pulse energy, the measured fluorescence signal with beam squeezing could be enhanced by three orders of magnitude with significant increase of the signal stability (see Fig. 3). This was ascribed to the more effective usage of the background energy in the smaller diameter beam [88]. With this understanding, an approach of merging the multiple filaments into a geometrical focus by using a telescope was developed to enlarge the initial diameter of the laser beam and thus the hot spots in the beam profile that may induce early self-focusing at a short distance [80]. A more effective usage of the background energy in the smaller beam near the geometrical focus results in a consistent and strong nitrogen fluorescence signals [80]. Since multiple filaments mainly result from some hot spots in the beam profile due to the imperfect intensity distribution across the beam cross section, adaptive optics was introduced to modify the initial divergence of the laser pulse or correct the wavefront's aberrations for the control of multiple filaments [89, 94]. For example, by using adaptive optics, it was demonstrated that the onset position of the filament could be extended significantly and as a result, strong nitrogen signal at a distance as far as 90 meters was detected using 40 mJ laser pulses [89].

2.3. Femtosecond laser filamentation in adverse atmospheric weather

For atmospheric sensing, it is important to deliver the high laser intensity to a far distance even in an adverse weather conditions. It was demonstrated that filaments indeed have the ability to propagate in an adverse atmospheric environment such as fog and clouds better than a normal nonfilamenting laser beam [50−53]. This was attributed to the presence of the low-intensity energy reservoir surrounding the filament core [95−103]. It was found that the reservoir can contain up to 90% of the pulse energy [102], and thus when a filament in the propagation path was blocked by particles like water droplets, snow crystals and dusts with dimensions comparable to or slightly larger than the filament diameter, the energy in the reservoir would refill the filament core (replenishment) downstream [97–99]. The effect of energy reservoir on the formation of filaments was also observed by examining whether the filament would be terminated or not after the background energy is blocked [102, 103]. Indeed, the filamentation process is terminated immediately after the energy reservoir is blocked [102, 103].

3. Ionization and fragmentation of molecules in femtosecond laser fields

Ionization and fragmentation of molecules are fundamental interaction processes in intense femtosecond laser fields [1]. In particular, for polyatomic molecules containing hydrogen atoms (hydrocarbon) that are among the sources of the greenhouse effect in the atmosphere, fragmentation dynamics of these molecules is more complicated [104]. This would contribute to the mechanisms responsible for the fingerprint emissions of such molecules and complicate the analysis of the chemical reactions in the interaction zone. In this section, the fingerprint emissions of molecules induced by strong-field–molecule interaction in the atmosphere are discussed based on the understanding of strong-field–molecule interaction in atmospheric as well as in vacuum conditions.

3.1. Filament-induced nonlinear spectroscopy of molecules

The fluorescence emission from a filament was first shown for nitrogen molecules in air with clean spectra free of plasma continuum [43]. The clean FINS spectra of air (see e.g., the spectrum in Fig. 4a) may originate from two facts: on the one hand, free electrons in the filament are created mostly through direct multiphoton/tunnel ionization. They could not absorb more energy from laser photons through inverse Bremsstrahlung within the ultrashort pulse [14, 105], giving rise to a low plasma temperature

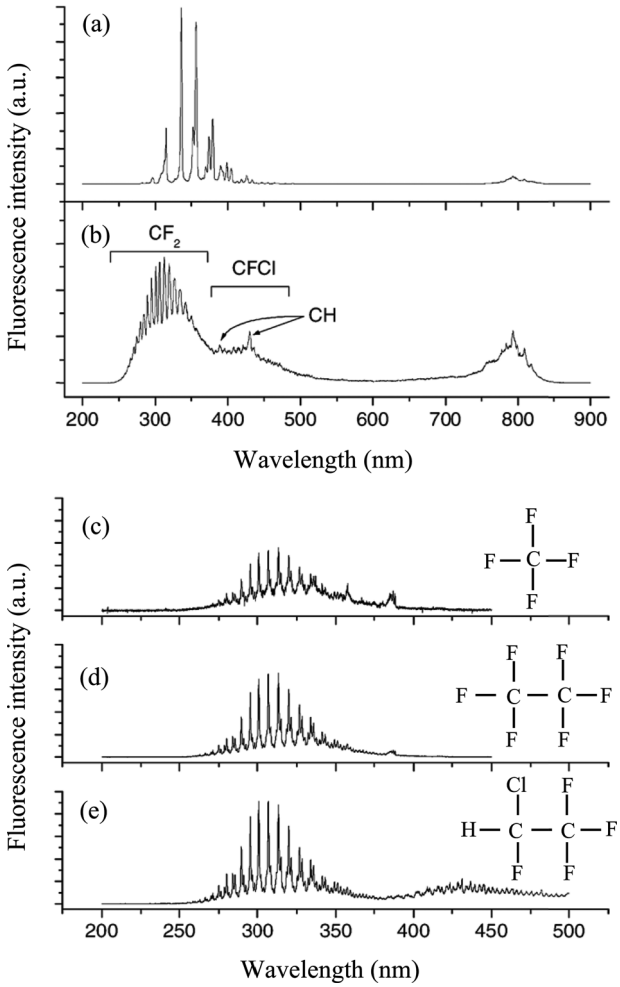

Figure 4 Spectra obtained for filament-induced fluorescence: (a) air; (b) HCFC-124. Laser pulse energy was 5 mJ, detector gate delay was set to 0 ns with respect to the pump laser, and gate width was 25 ns. (c–e) Time-gated fluorescence spectra for 25% halocarbon/air mixtures. Gate delay with respect to pump laser pulse was 10 ns, and gate width was 105 ns (with permission of Ref. [46]. Copyright 2004 American Chemical Society).

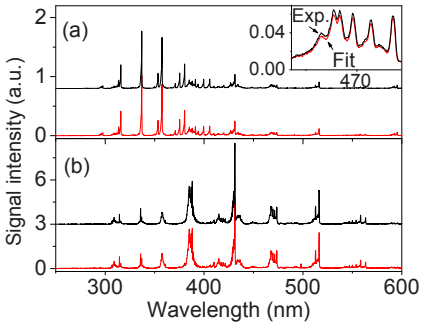

Figure 5 FINS spectra of air containing 1316 ppm of C_2H_2 and 5263 ppm of CH_4 measured with the time delays of (a) $t = -7$ ns (top) and (b) $t = +7$ ns (top) and their fits (bottom). The inset shows part of the experimental (exp.) and fitting (Fit) spectra with $t = -7$ ns in a higher resolution (with permission of Ref. [44]. Copyright 2007 AIP Publishing LLC.).

(~5800 K) [69, 105]; on the other hand, the dynamical balance between self-focusing and defocusing leads to a low plasma density ($\sim 10^{14}-10^{17}$ cm^{-3}) in air [67, 69]. It was observed that not only the FINS spectra of nitrogen molecules in air were clean, but also the fluorescence spectra from the fragmentation of fluorine-containing halocarbons, namely HCFC-124, CF_4 and C_2F_6, were clean (see e.g., the spectrum of HCFC-124 in Fig. 4b) [46]. Even when these molecules were mixed with air in a cell at atmospheric pressure, the fingerprint FINS spectra still kept clean, as shown in Figs. 4c and d, in which the nitrogen fluorescence was filtered out by time-resolved measurement based on the fact that the fluorescence lifetime of nitrogen molecules is much shorter than that of fluorescing fragments of halocarbons.

To show the ability of FINS for multicomponent sensing, simultaneous detection and identification of two unknown concentration targets (methane and acetylene) mixed with air at atmospheric pressure were performed using FINS when the fingerprint spectral database including the spectral signatures and the strengths of the signals of the corresponding trace species was already built [44]. By using a genetic algorithm the unknown spectra were well identified, as shown in Fig. 5. It was found that the detection sensitivity could reach ppm to ppb level, depending on the induced fluorescence efficiency from the molecules [44].

Remotely, optical emissions from nitrogen molecules in the filament have been extensively studied not only for the purpose of sensing [106], but also for characterizing remote plasma filaments [89, 107, 108]. To show the feasibility of FINS for atmospheric sensing, backward fluorescence of CH at 431 nm from methane mixed with air at atmospheric pressure in a tube was measured at a distance of a few meters, based on which the concentration sensitivity and the detection range limit were estimated to be the ppm level and kilometer range, respectively [109]. Backward fluorescence emission from ethanol vapor with a concentration of 0.8% was also measured in an open-air condition at a distance of 30 meters using a telescope system [110]. Furthermore, FINS of the mixture of CH_4, C_2H_2 and C_2H_4 in air was measured at 118 m distance with adaptive optics [111], illustrating the possibility to induce characteristic fluorescence at a remote place if the filament could be well controlled. FINS of a cloud of smoke produced from burning mosquito coils was also measured at a distance of 25 meters, in which CN, CH and C_2 molecular fragments were identified [112].

The feasibility of FINS for probing aerosols in air was examined as well. A cloud of microdroplets with dissolved table salt were measured in air with clear Na fluorescence observed at a distance of 16 m [113] and subsequently at a further distance of 70 meters [114]. Balmer hydrogen bands from the solvent of water were observed in the aqueous microdroplet cloud. Furthermore, well-resolved fluorescence emissions from a cloud of aqueous aerosols containing mixtures of $PbCl_2$, $CuCl_2$, $FeCl_2$ and NaCl were measured [115]. By controlling the filament using an adaptive optics,

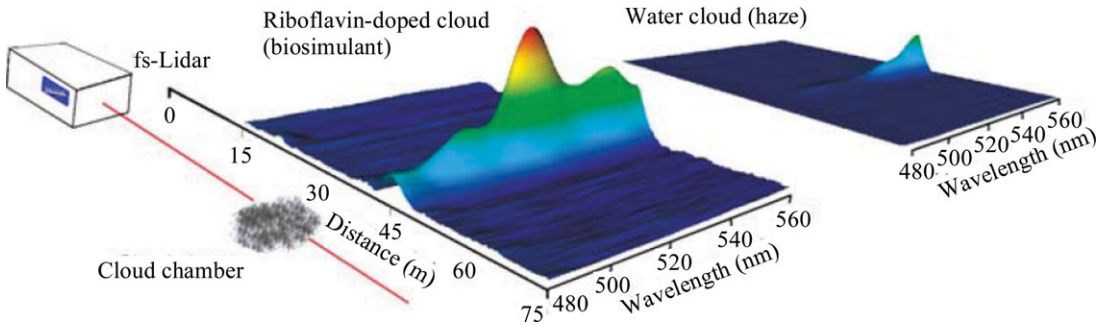

Figure 6 Remote detection and identification of bioaerosols. The femtosecond laser with the intensity of 10^{11} W/cm^2 illuminates a plume of riboflavin (RBF)-containing microparticles 45 m away (left). The backward-emitted two-photon-excited fluorescence, recorded as a function of distance and wavelength, exhibits the specific RBF fluorescence signature for the bioaerosols (middle) but not for pure water droplets (simulating haze, right) (with permission of Ref. [116]. Copyright 2004 Springer-Verlag).

FINS signals from the aerosol were demonstrated up to a distance of 118 meters [111]. A riboflavin-containing biological aerosol was also detected at a distance of 45 meters (Fig. 6) [116], in which the laser intensity in the interaction zone was, however, two orders of magnitude lower than the clamped intensity in an air filament in order to induce two-photon excited fluorescence of riboflavin.

3.2. Mechanisms for optical emissions of molecules in filaments

The underlying mechanisms behind the fingerprint emissions for air molecules including nitrogen and oxygen molecules in the plasma filament have been extensively studied [43, 63, 69, 117]. For molecular nitrogen, the fluorescence emissions from the first negative band system ($B^2\Sigma_u^+ - X^2\Sigma_g^+$ transition) of N_2^+ and the second positive band system ($C^3\Pi_u - B^3\Pi_g$ transition) of N_2 have been observed, as shown in Fig. 7. The mechanism of the optical emissions of nitrogen molecules in air filaments is now basically understood. The fluorescence emission of the first negative band system of N_2^+ was ascribed to intense laser-induced multiphoton/tunnel ionization of inner-valence electrons from the $\sigma_u 2s$ orbital of nitrogen molecules, leaving the molecular nitrogen ion in the excited $B^2\Sigma_u^+$ state [117]. This is an ultrafast process occurring within the laser pulse duration. While for the optical emission from the second positive band system of N_2, it may result, based on a pump-probe experiment [63], from the recombination of electrons with ions in the plasma filament through the collision reaction of $N_2^+ + N_2 \rightarrow N_4^+$ followed by the recombination with the electron ($N_4^+ + e \rightarrow N_2^* + N_2$), resulting in the excitation of the neutral excited state N_2^* ($C^3\Pi_u$), since the direct excitation between the ground singlet $X\,^1\Sigma_g^+$ and the excited triplet N_2^* ($C^3\Pi_u$) state is forbidden [43]. The simple recombination picture of electron and ions was ascribed to low plasma temperature and electron density in the air filament [69]. It was also argued that the excited state of N_2^* ($C^3\Pi_u$) may result from the electron impact in the plasma filament with higher electron

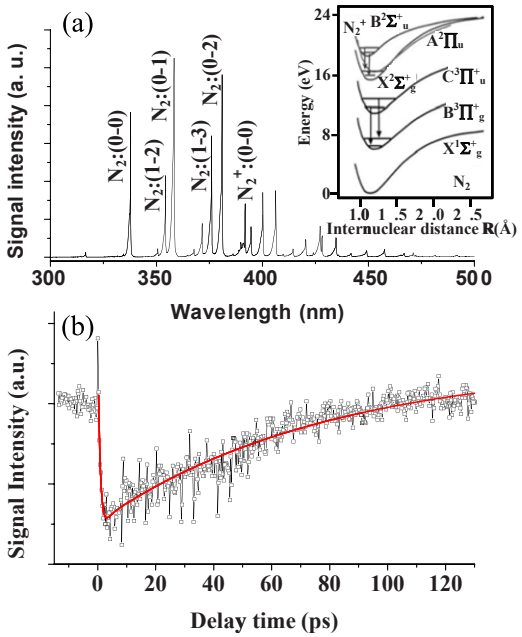

Figure 7 (a) FINS Spectrum from an air filament. Inset: energy diagram of nitrogen molecules for the optical emissions. (b) Signal intensity at 337 nm from the $C^3\Pi_u$ state as a function of the delay time between the 800-nm pump and 400-nm probe beams. The 800-nm pump beam is to create the plasma and populate $C^3\Pi_u$ state and the 400-nm probe is to kick the electrons from the $C^3\Pi_u$ state. The solid line represents the fit curve based on the rate equation including the collision and recombination processes (with permission of Ref. [63]. Copyright 2009 Elsevier B.V.).

density produced by the pulse with larger laser input energy [118, 119]. With the pump of a near-infrared light at 1053 nm, the forward lasing emissions at 337 nm, which corresponds to the $C^3\Pi_u$–$B^3\Pi_g$ transition, was observed (Fig. 8). Numerical calculations for the experimental condition of using 10-J, 8-ps long pulse result in a laser intensity spike in a femtosecond time scale that is followed by weak laser intensities with a slow decay of a few picoseconds. The latter heats the electrons and leads to the excitation of

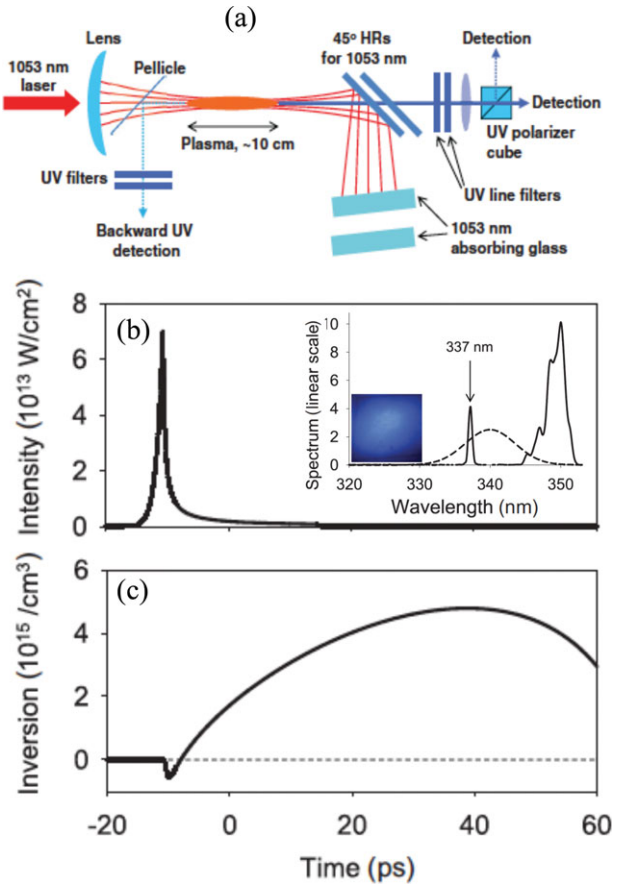

Figure 8 (a) Schematic of the experimental setup for generating the forward lasing emission at 337 nm; (b) the calculated time-dependent intensity of the 10-J, 8-ps pump pulse. The inset shows the spectrum of the forward-propagating UV optical signal and the photograph of the far-field intensity distribution of the third harmonic of the pump laser. (c) the population inversion on the 337-nm transition of nitrogen (with permission of Ref. [119]. Copyright 2013 American Physical Society).

neutral nitrogen molecules to the $C^3\Pi_u$ state by the impact of hot electrons.

For molecular oxygen, the emissions from the atomic transitions $2s^22p^3(^4S^0)3p$- $2s^22p^3(^4S^0)3s$ of oxygen atoms at 777.19, 777.42 and 777.54 nm were observed [69]. The intensity ratio of the individual peaks is close to 7:5:3, which is consistent with the ratio of the statistical weights of the upper levels of the transitions. The atomic oxygen in the plasma filament may result from the recombination of electrons and oxygen ions, and subsequent dissociation of oxygen molecules to atomic oxygen lying on the excited levels. Another possible scheme for the fluorescence emission of atomic oxygen may originate from the neutral dissociation of oxygen molecules via superexcited states (SESs), i.e., states beyond the ionization limit, created by multiphoton/tunnel excitation [120].

However, the mechanisms of the optical emissions for polyatomic molecules in the plasma filament in ambient air are quite complicated because the two successive processes of direct ionization and fragmentation of molecules induced by the high intensity of $10^{13}-10^{14}$ W/cm^2 and the collision interaction of the resultant ions/fragments with surrounding particles in air could not be resolved easily. Therefore, the investigation of strong-field–molecule interaction in atmospheric as well as in vacuum environments is generally required to explore the full picture of the fingerprint emissions of molecules in strong laser fields.

The fluorescing fragment of CH has been observed for a variety of hydrocarbon molecules in a plasma filament [44, 47, 48, 109, 110]. One of the possible schemes for the fluorescence emission was attributed to the neutral dissociation of parent molecules via SESs (superexcited states) (see Fig. 9a), which was confirmed experimentally by a pump-probe measurement [59]. When an infrared 1338 nm laser was used as the probe, an unambiguous reduction of the CH fluorescence signal coming from the dissociation of CH_4 was observed. This was ascribed to the de-excitation of the superexcited states of CH_4 by the probe laser pulse. The lifetime of the superexcited state of CH_4 was measured to be about 160 fs, as shown by Fig. 9b. It should be noted that the excitation picture depicted in Fig. 9a has been improved recently by including the phenomenon of population trapping [121] during high-field interaction. A brief description will be given later in Section 3.3.

On the other hand, it is possible that the fluorescing fragments of hydrocarbon molecules could come from the collision of resultant fragments with surrounding particles or the recombination of the resultant fragments with electron and subsequent dissociation of molecules [63, 109]. For example, the fluorescing emission from C_2 has been observed in an air/methane mixture plasma filament [109]. Since the C-C bond structure does not exist in the methane molecule, the fluorescing fragment of C_2 must come from some collision and dissociation reactions in the plasma filament such as the recombination reaction of electrons with the ionized CH_4^+ and CH_3^+, which has been observed in the interaction of methane molecules with strong femtosecond laser pulses [122]. Therefore, to get insights into the underlying mechanism for the fluorescing fragments, the dynamical reactions of molecules in intense laser fields have to be investigated.

Since fragmentation reactions of polyatomic molecules are essential building blocks of chemistry, many studies regarding the fragmentation of molecules in intense laser fields have been performed so far [104]. Earlier investigations on fragmentation of triatomic molecules such as CO_2 [123] and CS_2 [62] in intense laser fields have unveiled the large deformation of their skeletal structure along both the bending and the stretching coordinates. Furthermore, the high intensity achieved inside the filament would provoke, apart from single and multiple ionization and Coulomb explosion, hydrogen migration. This would give rise to new fragments that lead to more complicated reactions in the atmosphere. To show the complexity, below we will only give one example regarding the fragmentation of allene (CH_2CCH_2) in intense laser intensities of $10^{13}-10^{14}$ W/cm^2 by using the CMI technique [124]. The readers can refer to a few specific reviews that describe the current

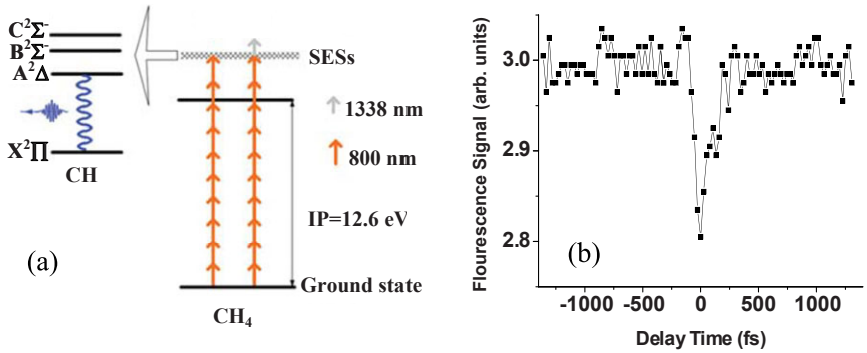

Figure 9 (a) Schematic scheme for the neutral dissociation of CH_4 and (b) fluorescence signal of CH at around 431 nm versus the delay time between the pump and probe pulses (with permission of Ref. [59]. Copyright 2008 IOP Publishing).

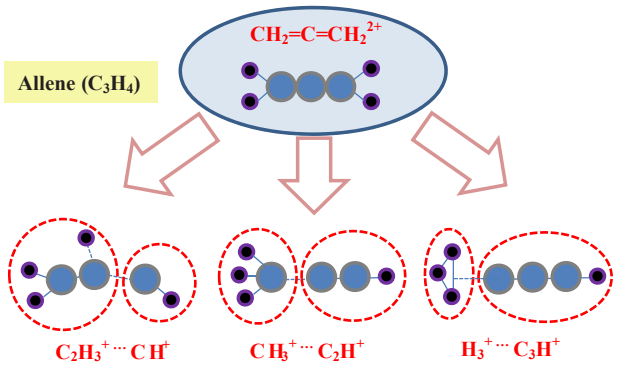

Figure 10 Schematic diagram for three fragmentation channels of C_3H_4 in an intense laser field. The observation of H_3^+, CH_3^+, and $C_2H_3^+$ implies that intramolecular hydrogen migration proceeds.

progress of ionization and fragmentation of molecules in intense laser fields [125–127].

For allene [124], the two channels $C_3H_4^{2+} \rightarrow CH^+ + C_2H_3^+$ and $C_3H_4^{2+} \rightarrow CH_3^+ + C_2H^+$ were unambiguously identified in an intense laser field (intensity: 2×10^{13} W/cm^2) by the CMI method [62, 128, 129], which demonstrated that structural deformation of the C−C−C skeleton occurs because of the migration of the hydrogen atom in C_3H_4 (see e.g., the decomposition channels of C_3H_4 shown in Fig. 10). Formation of H^+, H_2^+ and H_3^+ through two-body Coulomb explosion of allene was also identified [124]. The three-body Coulomb explosion of allene ($CH_2 = C = CH_2$) induced by an intense laser field (intensity: 4×10^{13} W/cm^2) was further analyzed in order to investigate the fragmentation dynamics [130], in which it was shown that the decomposition proceeds in a stepwise manner as well as in a concerted manner based on the kinetic energy distributions of the fragment ions produced through the two-/three-body Coulomb explosion pathways, $C_3H_4^{3+} \rightarrow H^+ + CH^+ + C_2H_2^+$ and $C_3H_4^{3+} \rightarrow H^+ + C_2H^+ + CH_2^+$, as well as the proton maps of both pathways.

The above example clearly shows the complexity of molecular fragmentation. The intensity range of an air filament under various focusing condition is between 5×10^{13} to $\sim1\times10^{14}$ W/cm^2 [65−68]. Many complex hydrocarbon molecules could be fragmented in such intensities as the above example of allene shows. This indicates that much more effort is needed to understand the fingerprint emissions of molecules in the intense laser fields in an air filament for environmental sensing. Meanwhile, more theoretical work is needed to elucidate the detailed physical processes of the interesting phenomena of ultrafast laser interaction with molecules.

3.3. Control of fragmentation of molecules in intense laser fields

Although FINS could be used as a fingerprint for identifying trace gases in the atmosphere at a far distance, the detection sensitivity is limited by the efficiency of generation of the fluorescence. Therefore, it is of particular interest in seeking a feasible strategy to enhance the yields of excited fragments of molecules induced by intense laser fields. For the fluorescence emissions from nitrogen molecules, it was experimentally demonstrated by using a pump-probe method that controlling the fluorescence emission of nitrogen molecules in an air filament is feasible [121], in which an obvious enhancement or reduction of the filament-induced fluorescence signals of nitrogen molecules at 391 (N_2^+) and 337 nm (N_2) can be realized when a blue (400 nm) or an infrared (1338 nm) laser pulse is used as the probe. The completely opposite effect was ascribed to the excitation enhancement of ionization and population trapping [121 and references therein] of some highly excited states including Rydberg states of nitrogen molecules, showing the possibility of controlling the fluorescence emission by designing laser pulses.

However, the realization of efficiently controlling of FINS of nitrogen molecules is based on the well-established understanding of the underlying mechanism behind the optical emissions of nitrogen molecules in strong laser fields. For polyatomic molecules, the studies are still at the very fundamental stage by investigating the fragmentation of molecules in intense laser fields in vacuum conditions [126, 131–134]. Controlling the chemical reaction dynamics of hydrocarbon molecules with different methods, such as chirping the intense laser pulses [131], modifying the pulse width and wavelength [132], adjusting the pulse intensity and polarization [133, 134], have been carried out.

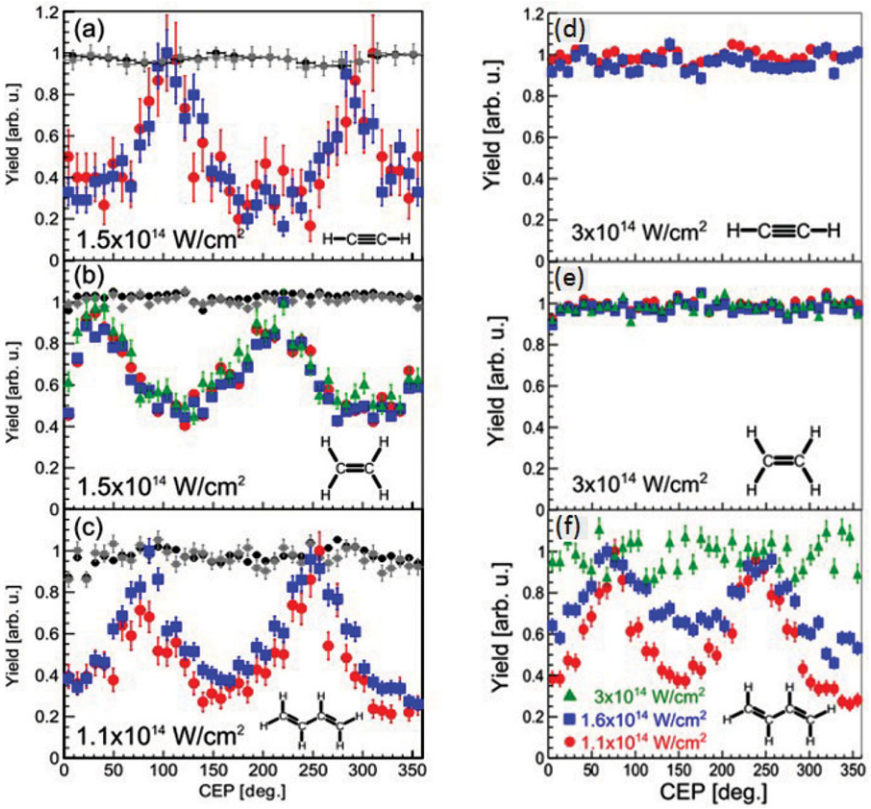

Figure 11 (a)–(c) Measured fragmentation yields as a function of CEP for different channels of (a) acetylene, (b) ethylene and (c) 1,3-butadiene, measured at the laser intensities indicated in the panels. The channels are $C_2H_2^{2+} \rightarrow CH^+ + CH^+$ (red dots) and $C_2H_2^{2+} \rightarrow H^+ + C_2H^+$ (blue squares) for acetylene in (a); $C_2H_4^{2+} \rightarrow CH_2^+ + CH_2^+$ (red dots), $C_2H_4^{2+} \rightarrow H^+ + C_2H_3^+$ (blue squares), and $C_2H_4^{2+} \rightarrow C_2H_2^+ + H_2^+$ (green triangles) for ethylene in (b); $C_4H_6^{2+} \rightarrow C_2H_3^+ + C_2H_3^+$ (red dots) and $C_4H_6^{2+} \rightarrow CH_3^+ + C_3H_3^+$ (blue squares) for 1,3-butadiene in (c). The ionization yields of the singly and doubly charged molecular ions are denoted by black dots and gray squares, respectively. (d), (e) Fragmentation yields over the CEP of the same channels as in (a) and (b), but measured for a slightly higher intensity (as indicated). (f) Measured intensity dependence of the yield of the fragmentation channel $C_4H_6^{2+} \rightarrow CH_3^+ + C_3H_3^+$ over CEP. The laser intensities are indicated in the figure (with permission of Ref. [9]. Copyright 2012 American Physical Society).

As an example, efficient control over various fragmentation reactions of a series of hydrocarbon molecules including acetylene, ethylene and 1,3-butadiene by the optical waveform-controlled intense few-cycle laser pulses was experimentally demonstrated recently by using the CMI method, as shown in Fig. 11 [9]. For more information about the ionization and fragmentation of molecules in intense laser fields, the readers can refer to the available reviews [104, 125–127].

3.4. Application to atmospheric science

The feasibility of femtosecond laser ionization and fragmentation of molecules through filamentation for sensing application has been shown in Section 3.1 by demonstrating fingerprint FINS spectra for air molecules, trace hydrocarbon molecules and aerosols in ambient atmosphere. In this section, we introduce two examples by using the FINS technique for atmospheric humidity measurement [135, 136], which is an important issue in atmospheric science because it reflects the changes of water concentration in the atmosphere. In addition, filamentation-assisted water condensation has been recently demonstrated both in a cloud chamber and in the atmosphere [29–31, 137, 138], as presented in Fig. 12 as an example, in which filament-induced water vapor condensation was shown by measuring the scattering light from the generated water droplets in a subsaturated chamber [29]. Therefore, the humidity measurement would also be helpful for understanding the water condensation condition and the physics in cloud formation or even lightning control in the atmosphere.

Shown in Fig. 13a is the clear FINS spectrum of water vapor in the spectral range of 306–309 nm when a filament was formed above a conical flask filled with distilled water [135]. OH radical was identified, which was ascribed to the dissociation of water vapor molecules in air. Typical nitrogen fluorescence from the filament in air was also observed. It was found, as shown in Fig. 13b, that the closer the filament was to the water surface, the stronger the OH fluorescence. This is because the water vapor partial pressure in air is related to the distance to the water surface, which follows an exponential decay as shown by the fit (red line) in Fig. 13b. When the vapor partial pressure decreases to the partial pressure in the room, the signal remains constant, as indicated by the blue dash line in Fig. 13b. Figure 13c shows the water-temperature dependence of the filament-induced fluorescence of water vapor with a fixed distance between the filament and the water surface. It can be seen that when the water temperature increases, the water vapor concentration first increases, leading to the stronger OH fluorescence, but as the temperature increases to a certain value, the OH fluorescence reaches a constant value, indicating that the vapor concentration reaches saturation. It was demonstrated as shown in Fig. 13d that the vapor partial pressure is linearly proportional to the fluorescence signal of water vapor. This result provides a significant way to measure absolute humidity by monitoring water vapor fluorescence inside a filament.

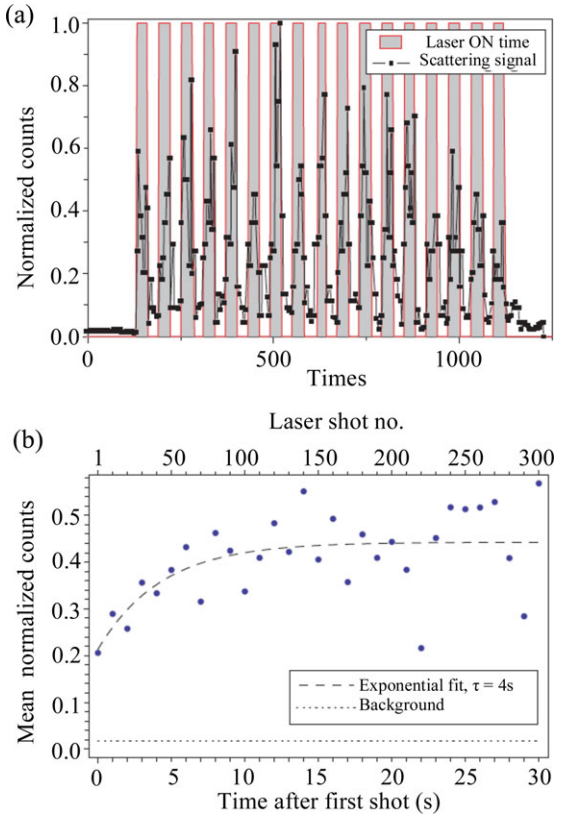

Figure 12 Filament-induced water condensation in a subsaturated atmospheric cloud chamber ($T = 60$ °C, relative humidity = 75–85%) observed through the scattered-light signal. (a) High reproducibility of the effect over repeated laser on/off cycles; (b) Rise time of the light scattered by the growing droplets. (with permission of Ref. [29]. Copyright 2010 Nature Publishing Group).

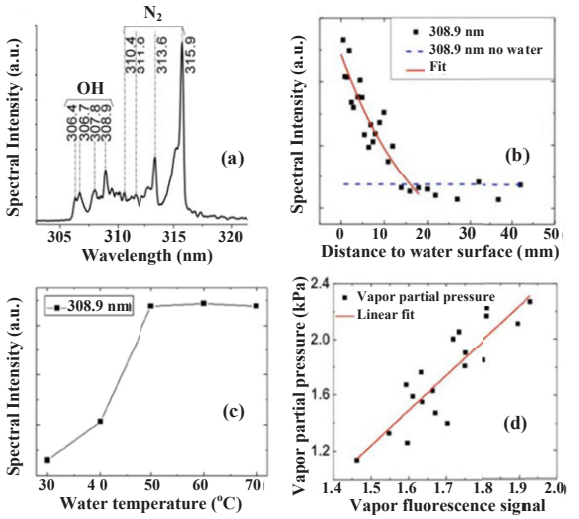

Figure 13 (a) Typical FINS spectrum of water vapor in air in the range of 303–322 nm; (b) signal intensity of OH at 308.9 nm as a function of the distance between the filament and water surface with water temperature at 21 °C. Blue dashed lines indicate the spectral intensity when the water container was removed from the interaction zone. Red solid line is exponential fit. (c) Water temperature dependence on fluorescence intensity of 308.9 nm OH radical; (d) partial pressure of water vapor in air as a function of OH signal at 308.9 nm (with permission of Ref. [135]. Copyright 2012 Optical Society of America).

However, the 308.9-nm fluorescence line from hydroxyl (OH) radical arising from laser-induced dissociation of water vapor is rather weak (two orders of magnitude weaker than nitrogen fluorescence at 337 nm), and thus cannot be easily detected meters away. Another FINS experiment was carried out to detect the humidity by using the strong fluorescence emissions from nitrogen monohydride (NH) free radical at 336 nm, which was produced from an intense blue (400 nm) filament [136]. The experimental results showed that the fluorescence from NH free radicals is linearly dependent on the relative humidity in air. The generation mechanism of the fluorescing NH radical is still not totally clear, but it might result from complicated collisional processes of the dissociated N_2 and water-vapor molecules in the air filament.

3.5. Application to combustion science

Sensing combustion intermediates is of particular importance to rationalize the physical and chemical nature of combustion systems for efficient combustion with low-pollution products. Since femtosecond laser filamentation can be formed with less perturbation in adverse atmospheric conditions, it would be advantageous to combustion diagnostics for the highly turbulent combustion environment. Recently, the feasibility of FINS for combustion diagnostics was demonstrated, in which the laminar ethanol−air flame on an alcohol burner was employed as the target because of the similarity of its diffusion to other practical systems such as rocket combustor and industrial stoves [19, 139, 140].

Figure 14a shows a typical FINS spectrum of the ethanol−air flame in ambient atmosphere [19]. The filament was formed at a height of 17 mm (dashed line D) above the burner wick (dash line O), as shown by the inset (I) in Fig. 14a. The spectral bands were assigned to the Swan band ($d^3\Pi_g$-$a^3\Pi_u$) and the Deslandres-D'azambuja band of the C_2 radical, the $A^2\Delta$-$X^2\Pi$ and $C^2\Sigma^+$-$X^2\Pi$ transitions of the CH radical, and the $B^2\Sigma^+$-$X^2\Sigma^+$ transition of the cyano radical CN [19]. In addition, several weak band emissions from the molecules such as N_2 (337 nm), NH (336 nm) and OH (307 nm) and atomic carbon lines at 247.7 nm and H_α at 656 nm were also recognized in Fig. 14a. The identification of these free radicals and atomic species in the flame confirms the potential of FINS for detecting the intermediate species in a combusting flow by the femtosecond filament excitation.

The ability of FINS in mapping the concentration distribution of combustion intermediates in flames was also demonstrated by measuring FINS spectra at different

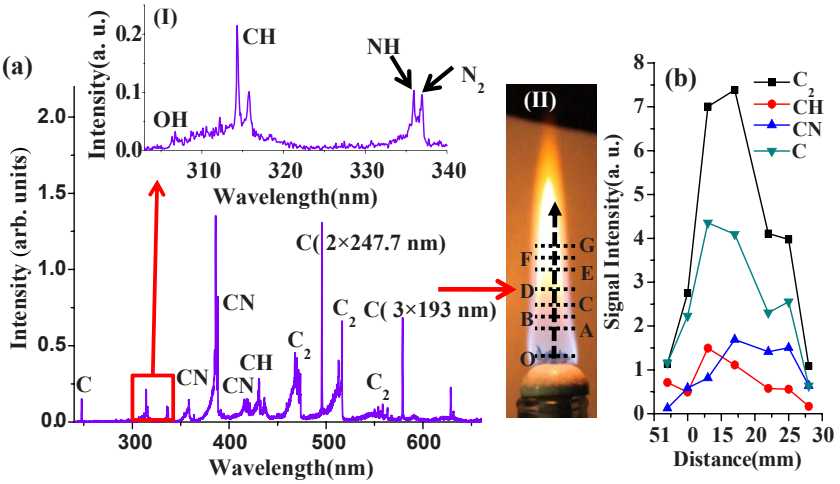

Figure 14 (a) Spectrum of the ethanol–air flame on an alcohol burner by the femtosecond filament excitation. (b) Signal intensities of C_2, CN C, and CH obtained at different positions of the flame. Insets in (a): (I) zoomed-in spectrum in the range of 303–340 nm; (II) picture of the flame and the filament positions marked by the dashed lines (with permission of Ref. [19]. Copyright 2013 Optical Society of America).

positions of the flame along the dashed-arrow line of the inset (II) in Fig. 14a. The signal intensities of the four species, C_2, CH, CN and C, as a function of the distance are shown in Fig. 14b, from which it can be seen that the signal intensities from all the four species first increase and then decrease as the distance increases, reflecting the concentration distribution of the four intermediate species in the flame.

4. Remote lasing actions by femtosecond laser pulses

One of the main tasks in developing remote laser sensing techniques is to enhance the signal-to-noise ratio and improve the detection sensitivity. Therefore, if the optical emissions of FINS could undergo amplification, it would be advantageous to sensing applications. Indeed, recent observations of backward and forward lasing actions during filamentation in air [33–37, 118, 119, 141–146] and in other gases [54, 55, 147, 148] have indicated a distinct enhancement of signal intensity, and also a unique free-space amplified light source, inspiring strong interest in the development of remote lasers for atmospheric applications. In this section, we will overview the recent progress in remote lasing actions driven by femtosecond laser filamentation.

4.1. Remote amplified spontaneous amplification

Amplified spontaneous emission (ASE) along the direction of the plasma filament was first observed in 2003 by detecting the backscattering nitrogen fluorescence [33]. It was shown from the detection of the backward scattered fluorescence that the fluorescence intensity of N_2 at 337 and 357 nm from the transition of $C^3\Pi_u \rightarrow B^3\Pi_g$ increases exponentially as the filament length increases. The population inversion for the nitrogen ASE lasers was initially ascribed to the recombination of free electrons with ions in the plasma. Subsequently, by using an infrared femtosecond laser pulse (3.9 m or 1.03 m) inside a gas mixture of argon and nitrogen, backward ASE at 337 nm and 357 nm were observed [141]. The population inversion mechanism between the $C^3\Pi_u$ and $B^3\Pi_g$ states was attributed to the traditional Bennett mechanism, where collisions transfer the excitation energy of argon atoms to molecular nitrogen. An ASE laser has also been shown with oxygen molecules as the gain target by using a 226-nm, 100-ps laser as the excitation source, which drives the dissociation of molecular oxygen followed by two-photon resonant excitation of the resulting atomic oxygen fragments (Fig. 15) [149]. But the UV excitation light is rather weak and encounters the difficulty to project over a long distance due to the atmospheric absorption.

Recently, by using circularly polarized femtosecond pulses of a typical 800-nm Ti:sapphire laser with a pulse energy of ~10 mJ, a strong backward ASE lasing signal at 337 nm was obtained [118]. It was shown that the presence of oxygen molecules in the mixture of nitrogen and oxygen gas suppresses the lasing action to a large extent. The mechanism of population inversion was attributed to inelastic collisions between electrons and neutral nitrogen molecules, which is more efficient when circularly polarized laser pulses are used. A multiple-pulse scheme for the remote atmospheric ASE lasing was also proposed, which relies upon a pulse train to boost the plasma density in the seed channel to satisfy the transient population inversion for amplification [150]. Theoretical simulations on the possible mechanisms were reported as well [151–153].

Moreover, ASE has been demonstrated for air–hydrocarbon mixtures [54] and water vapor [148]. For the air–hydrocarbon mixture (i.e. CH_4, C_2H_2, and C_2H_4), backward emission from the neutral fragment of CH at one atmospheric pressure was measured, which showed the exponential dependence on the filament length, indicating the existence of ASE. The neutral fragments were ascribed to the neutral dissociation of the parent hydrocarbons via SESs inside the filament [60]. For water vapor in air, experimental observation of ASE was first shown with the

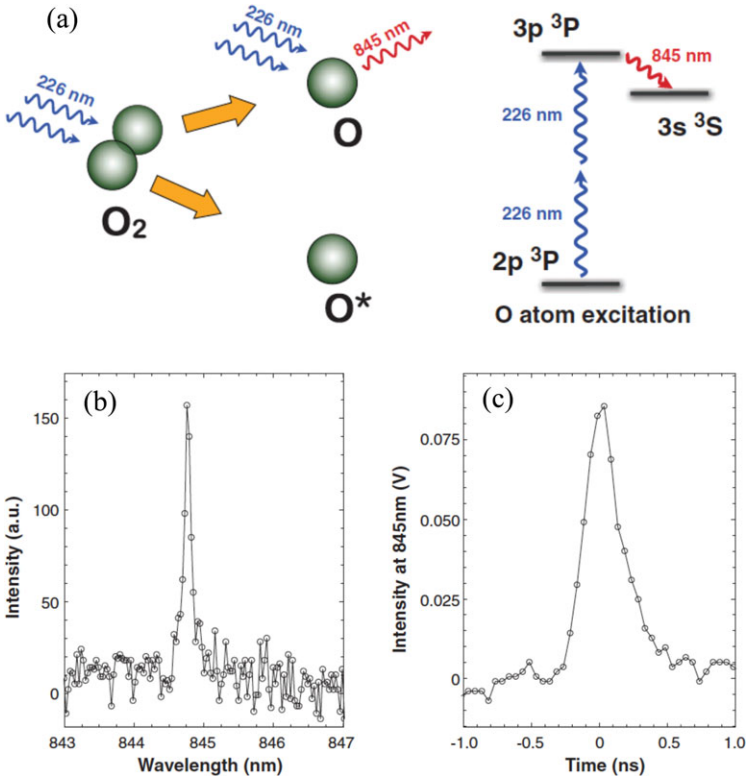

Figure 15 (a) Schematic diagram for the generation of ASE lasing of atomic oxygen at 845 nm pumped by an 226-nm, 100-ps laser pulse; (b) backscattered spectrum and (c) pulse duration of atomic oxygen emission (with permission of Ref. [149]. Copyright 2011 The American Association for the Advancement of Science).

fluorescing hydrogen monoxide (OH) fragmented from water molecules [148]. The backward OH signal increases exponentially as the filament length increases. The lasing action was also linked to the SES dissociation process of H_2O molecule in intense laser fields [148]. Furthermore, it was shown on water vapor that the backward fluorescence of NH in the mixture filament also follows an exponential increase with increasing filament length, indicating the ASE action, but the detailed underlying physics for the establishment of population inversion of NH in the mixture of water vapor and air though filamentation is still unclear [136].

The generation of lasing action in the laminar ethanol−air flame on an alcohol burner array was recently demonstrated using femtosecond filament excitation for combustion diagnosis [55]. By probing the backward emissions of combustion species, it was found that as the interaction length of the filament in the flame increases, the signal intensity for the $B^2\Sigma-X^2\Sigma$ transition of CN at 388 nm increases exponentially. However, the C_2 emissions from the $A^3\Pi_g$–$X'^3\Pi_u$ transition at 474 nm shows a linear dependence on the interaction length of the filament inside the flame, as shown in Fig. 16. The exponential behavior of the CN emission was ascribed to the occurrence of ASE, which provides a way to overcome the quenching effect of specific species for combustion diagnosis.

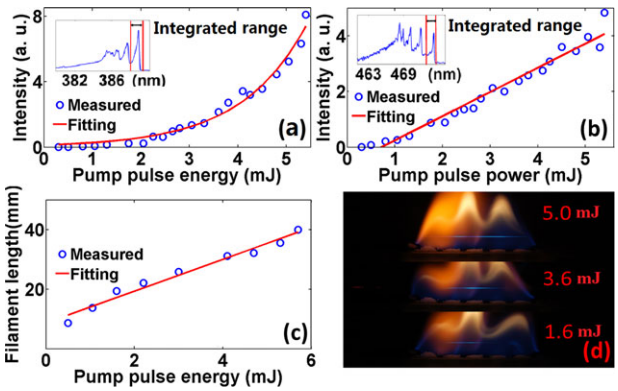

Figure 16 Measured (circle) and fitted (solid line) dependence of (a) the emission intensity of CN at 388 nm and (b) that of C_2 at 474 nm on the input laser energy. Insets in (a) and (b) show the integrated range of spectrum for obtaining the signal intensities of CN and C_2, respectively. (c) The measured (circle) and fitted (solid line) plasma lengths in the flame versus the input laser energy. (d) The photos of the flame together with the filament taken for three incident laser energies (with permission of Ref. [55]. Copyright 2014 AIP Publishing LLC).

4.2. Remote self-induced seed amplification

Recently, a self-induced seeding laser scheme was demonstrated from N_2^+ in an air filament pumped by intense mid-infrared pulses [34]. In this scheme, by using self-generated harmonics of the infrared femtosecond pump laser during filamentation as the seed, forward and switchable multiwavelength remote laser in air was realized, as shown in Fig. 17. The lasing wavelengths correspond to different vibrational transitions between the $B^2\Sigma_u^+$ and $X^2\Sigma_g^+$ states of N_2^+. The pulse duration of such remote lasers was

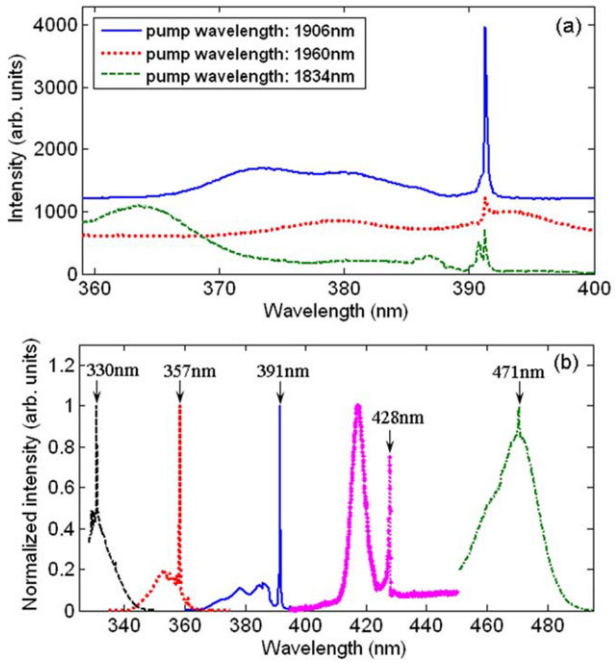

Figure 17 (a) Measured spectra of remote laser at 391 nm for different pump wavelengths of 1834, 1906, and 1960 nm showing the lasing is sensitive to the pump laser wavelength; (b) the lasing peaks at 471, 428, 391, 357, and 330 nm achieved with different pump wavelengths of 1415, 2050, 1920, 1760, and 1682 nm, respectively. Curves are shifted vertically in (a) for clarity (with permission of Ref. [34]. Copyright 2011 American Physical Society).

measured to be in sub-10-ps range [142]. The establishment of the population inversion in N_2^+ was suggested to be very fast with a sub-ps time scale because the self-generated harmonics have pulse durations comparable to the pump laser. This self-induced seeding laser scheme is fundamentally different from the above-mentioned ASE lasers, which are based either on electron−ion recombination or electron impact with a ps−ns time scale for the establishment of population inversion.

To verify the population inversion mechanism, the self-generated-harmonic-seeded laser was investigated in different gas mixtures, i.e., N_2−Ar, N_2−Xe and N_2−Ne [143]. It was found that all the laser signals obtained in these mixtures follow the small-signal gain equation, suggesting that population inversion, rather than nonlinear processes such as four-wave mixing and stimulated Raman scattering is the most likely mechanism. The "instantaneous" population inversion in N_2^+ was ascribed to nonlinear excitations of the ionic N_2^+ system in the filament [142, 154]. This is because neutral nitrogen molecules in the ground state could not be directly excited to result in the population inversion of N_2^+ through highly nonlinear processes such as multiphoton or tunnel ionization due to the lower ionization rate of the excited $B^2\Sigma_u^+$ state than that of the ground $X^2\Sigma_g^+$ state. However, because the high intensity of the order of $10^{13}-10^{14}$ W/cm^2 is reached within the ultrafast pulse duration as filamentation and ionization take place, the ground molecular ions would experience the high intensity inside the filament once it is created, leading to the population inversion of N_2^+ through lower-order multiphoton processes with very high efficiency [154]. This process may be universal in a femtosecond laser filament in different gases such as CO_2 [147]. However, the establishment of population inversion is still not totally clear. For example, it was demonstrated that the signals of air lasers at 391 nm and 428 nm, which respectively correspond to the (0–0) and (0–1) vibrational transitions between the $B^2\Sigma_u^+$ and $X^2\Sigma_g^+$ states of N_2^+, showed different behaviors when the polarization of the pump laser evolves from linear to circular [155]. In addition, under low pressures at tens of mbar, superradiance owing to the quantum coherence via cooperation of an ensemble of excited N_2^+ molecules may dominate the forward emissions when the dephasing time is long enough [156].

4.3. Self-lasing in air using only one laser source

Since the temporal and spatial overlapping of two pulses over a long distance is particularly difficult, the generation of lasing actions by using a two-beam scheme in a femtosecond laser filament is not practical for remote application. Therefore, producing a coherent amplification light source in free space with only one femtosecond laser beam would be very advantageous. As introduced in the above section, by using only one infrared pump laser light at ~1.9 μm, remote forward laser actions can be realized [34], but the limited output energy of the infrared laser pulse from the optical parametric amplifier (OPA) makes it hard to generate a filament at a far distance. It is therefore expected that the generation of remotely coherent lasers could be realized directly by using commercially available high-power Ti:sapphire laser systems with the wavelength at 800 nm [35, 36, 144, 145, 157].

By using the white-light (supercontinuum) generated during the filamentation in air as the seed, the remote self-seeding laser amplification by using only one 800-nm Ti:sapphire femtosecond laser pulse was achieved almost at the same time by several groups [35, 36, 144]. The self-induced narrowband laser at 428 nm has a pulse duration of ~2–3 ps with perfect linear polarization property, but the lasing emission shows a doughnut pattern, as shown in Fig. 18 [36]. The self-induced-white-light-seeded lasing action can be strongly influenced by external focusing conditions [145]. It was shown that the self-seeded lasing signal of N_2^+ at ~391 nm decreases dramatically by orders of magnitude and ultimately disappears when the focal length of an external lens increases from 0.5 m to 1 m. By using telescope optics to optimize the filamentation at a remotely designated distance, the distance of lasing action was extended significantly, providing possibilities for

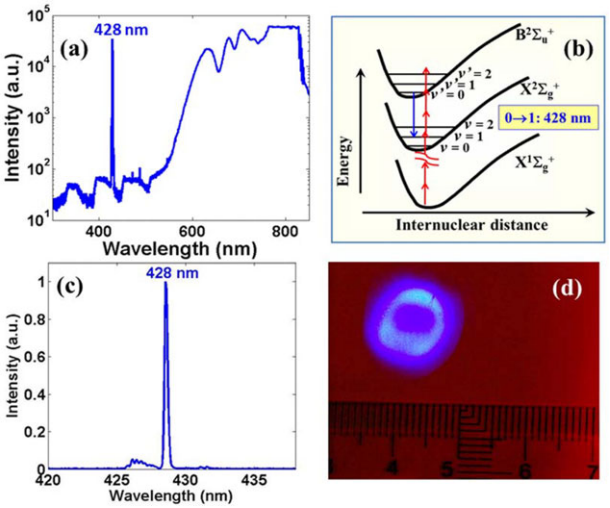

Figure 18 (a) Experimentally measured spectrum of supercontinuum with the strong narrowband emission at ~428 nm. (b) Energy-level diagram of ionized and neutral nitrogen molecules in which the vibrational transition between the $B^2\Sigma_u^+(v=1)$ and $X^2\Sigma_g^+(v=0)$ states corresponding to a 428 nm wavelength is indicated. (c) Experimentally measured spectrum of the lasing emission at 428 nm separated from the supercontinuum spectrum. (d) Far-field profile of the 428 nm laser pulse (with permission of Ref. [36]. Copyright 2014 IOP Publishing).

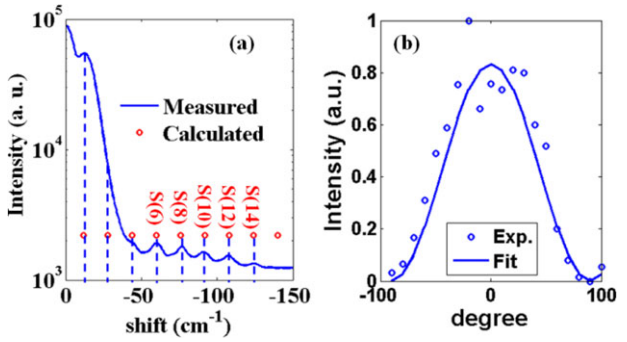

Figure 19 (a) Measured Raman spectrum (blue solid) induced by intense lasing emission at 428 nm, and calculated Raman peaks in neutral nitrogen with a rotational constant $B_e = 1.998$ cm^{-1} (red circle). (b) Measured polarization property of the Raman signals (blue circle) fitted by $\cos^2\theta$ (blue solid) (with permission of Ref. [158]. Copyright 2014 Optical Society of America).

practical applications of remote lasing in standoff spectroscopy [145].

Based on the white-light seeding scheme, lasing emissions at 428 nm with a maximum output energy of 2.6 μJ and a maximum conversion efficiency of 3.5×10^{-5} at the distance of 1 m was demonstrated recently [37]. The optical gain inside the filament plasma was estimated to be in excess of 0.7/cm. It was found that the lasing emission increases rapidly over a small range of pump laser power followed by saturation, which was attributed to the defocusing of the seed in the plasma amplifying region and to the saturation of the seed intensity. A self-induced nitrogen laser at 337 nm in the forward direction was also shown with the pump of 10-J, 1053-nm, linearly polarized, picosecond laser pulses. In this case, the self-generated third harmonic served as the seed [119]. However, it was demonstrated that the 337-nm nitrogen laser can only be observed when the pump pulse is longer than 2 ps. In combination with the numerical simulation, it was pointed out that only when the pump pulse is long enough, can electrons be sufficiently heated by the laser field, which is capable of the population inversion of N_2 through electron-impact excitation [119].

4.4. Application of remote lasers

Based on the above discussion, it can be seen that the lasing actions in air can greatly enhance the signal intensities of the optical emissions in an air filament, providing the possibility for future practical applications. Interestingly, besides providing a way to enhance the detection sensitivity for remote sensing, the air lasers could also act as a coherent, narrow bandwidth probing source [158]. It was demonstrated that by using the self-induced narrow bandwidth, intense sub-10-ps air laser as a probe, impulsive Raman scattering of nitrogen molecules can be remotely initiated inside a femtosecond filament with a conversion efficiency of up to ~0.8% [158]. As shown in Fig. 19a, the Raman peaks located in the spectrum with shift values larger than 50 cm^{-1} were well distinguished and spectrally separated. The polarization property of the Raman peaks was found to be almost perfectly linearly polarized with the direction parallel to that of the laser line, as shown in Fig. 19b. As pointed out in Ref. [158], this scheme provides two unique advantages. First, the pump and the probe pulses naturally overlap in both time and space, since the probe pulse is generated in the filament induced by the pump laser. Secondly, the femtosecond laser filamentation process offers the potential to realize Raman fingerprinting at a remote distance. Both these advantages are highly desirable for atmospheric sensing.

Recently, it was found that the air laser could be strongly affected by rotational wavepackets of molecular ions, based on which quantum coherence in the rotational states of the population-inverted molecular ions can be characterized [18]. In this experiment, by detecting the lasing actions of nitrogen molecules in the frequency domain, the coherent wave packet was mapped onto the frequency-resolved spectrum of the air laser. Periodic modulation of the laser signals stemming from the revivals of the coherent rotational wavepackets in the excited electronic states $B^2\Sigma_u^+$ were further exhibited in the time domain. From the application point of view, the fact that the rotational coherence can faithfully encode its characteristics into the amplified seed pulses suggests that the air laser can potentially provide a promising tool for remote characterization of coherent molecular rotational wavepackets.

5. Summary and outlook

In this overview we presented results of recent studies of the interaction of strong laser fields with molecules in air and demonstrate the feasibility to use femtosecond laser pulses to remotely ionize and fragment molecules for environmental sensing based upon the laboratory-scale demonstrations, which is still the current stage of this research field. When propagating in air, femtosecond laser pulses induce high intensity through filamentation, which can be actively controlled to occur at a far distance in adverse atmospheric conditions. The high intensity inside a filament leads to the ionization and fragmentation of molecules that emit light. It was demonstrated that the emitted light of molecules from inside the filament are characteristic fluorescence; i.e. there is practically no background plasma continuum and no atomic line emissions from the filament zone [43]. Only emissions from molecular bands of simple molecular fragments were observed, which are called "clean fluorescence". Progress has been further made in the identification of clean fluorescence from various substances, such as hydrocarbons, water vapor, and aerosols. The identification of the traces in a mixture of gases in the atmosphere was also demonstrated based on the spectral database built up from the measured clean fluorescence [44], which indeed shows the feasibility of femtosecond laser filamentation for environmental sensing through the ionization and fragmentation of molecules. A variety of schemes have also been developed to improve signal-to-noise ratios of the clean fluorescence by using, for example, two-color laser fields [121], and air lasing via amplified spontaneous emission [33, 149] and seed amplification [34]. The sensing scheme associated with femtosecond laser ionization and fragmentation of molecules is very promising because it provides the possibility to induce the fluorescence for a large number of molecular species of interest in the propagation path of filamentation with only one single laser. It also opens up a new way towards sensing "dark species", which emits light after ionization and fragmentation.

However, the practical application of this idea is still challenging and strongly depends on the progress of the understanding of strong-field–molecule interaction in atmospheric as well as in vacuum environments. Actually, the physical and chemical reactions involved in the interaction of molecules with the intense laser field inside the filament are only partially understood. The underlying mechanism of the clean fluorescence is not totally clear even for nitrogen molecules inside a filament in air, which has been long investigated. Therefore, the first challenge is essentially the understanding of the optical emissions of gaseous molecules and aerosols in the atmosphere. The second challenge in this field is the establishment of the complete spectral database including the spectral signatures and the strengths of the signals of the new specific species for practical applications. So far, the numbers of gaseous species included in the spectral database are very limited with several hydrocarbons, carbon dioxide and atmospheric major constituents, oxygen, nitrogen and water vapor. The third challenge is how to efficiently control the long propagation of the robust confined filamentary structures. Although kilometer-range filamentation has been shown [51], the longest distance of the clean fluorescence that has been measured is only ~100 meters [80, 111]. This is limited by the white-light noise generated during filamentation, which should be reduced significantly for practical applications.

In view of the complexity of ionization, fragmentations and collisions of molecules and molecular ions in strong laser fields in the atmosphere, all of which may affect the induced fluorescence emission, it is clear that much additional effort is needed to enhance the sensitivity, selectivity, and precision of this technique for environmental sensing applications. However, there is no doubt that the next few years will see exciting application of femtosecond laser ionization of molecules in environmental sensing. First, the rapid advance of powerful femtosecond laser technologies provides the possibility to better control the filamentation process and also remote lasing actions for improving the sensitivity of this sensing technique. Secondly, the further understanding of the basic physics and chemistry of FINS spectra would lead to the feasibility of the quantitative analysis of the concentration of specific species in filaments. Lastly, developing coherent dynamical control methods of optical emissions in filaments may enhance the selectivity of specific species for precision detection.

Acknowledgements. This work was supported in part by the National Natural Science Foundation of China (61427816, 61235003), the National Basic Research Program of China (2014CB921300), Research Fund for the Doctoral Program of Higher Education of China, Fundamental Research Funds of Jilin University. SLC acknowledges the support of the Natural Sciences and Engineering Research Council of Canada (NSERC), Canada Research Chairs, Canada Foundation for Innovation (CFI), The Canadian Institute for Photonics Innovation (CIPI) and the FQRNT.

Received: 29 August 2014, **Revised:** 23 February 2015, **Accepted:** 27 March 2015

Published online: 5 May 2015

Key words: Femtosecond laser, sensing, ionization and fragementation, molecules, stimulated emission.

Huailiang Xu received his PhD in Physics from Lund University of Sweden in 2004. He then worked as a postdoctoral researcher at Laval University of Canada. In January 2008, he became an assistant professor at The University of Tokyo, Japan. Since September 2009, He has been a full professor at Jilin University, China. His research interests have been ultrafast laser sensing, strong-field laser physics and atomic and molecular spectroscopy.

Ya Cheng is currently a professor of the Shanghai Institute of Optics and Fine Mechanics, Chinese Academy of Sciences. His research activity has mainly focused on ultrafast nonlinear optics. His current research interests include femtosecond laser micromachining of glass materials and ultrafast nonlinear optics in the tunnel ionization regime. He is currently an editor of J. Laser Micro Nanoengineering and Chin. Phys. Lett., and a Fellow of the Institute of Physics (UK).

See-Leang Chin received his PhD in Physics from University of Waterloo in 1969. He was appointed as a full professor at Laval University in 1982. He received the Humboldt Foundation's Research Award in 1999. He has held a Canada Research Chair (senior) since January 2001. In 2011, he was awarded the CAP medal for lifetime achievement in Physics from the Canadian Association of Physicists for his outstanding contributions to ultrafast intense laser science, which is his current field of research.

Hong-Bo Sun received his PhD in electronics from Jilin University in 1996. He worked as a postdoctoral researcher at University of Tokushima from 1996 to 2000, and then as an assistant professor at Osaka University. In 2005, he was promoted as a full professor (Changjiang Scholar) in Jilin University. He was awarded the Outstanding Young Scientist Award issued by the minister of MEXT (Japan) in 2006. His research interests have been laser nanofabrication and ultrafast spectroscopy.

References

[1] K. Yamanouchi, Science **295**, 1659–1660 (2002).
[2] R. Vellota, N. Hay, M. B. Mason, M. Castillejo, and J. P. Marangos, Phys. Rev. Lett. **87**, 183901(1–4) (2001).
[3] P. H. Bucksbaum, A. Zavriyev, H. G. Muller, and D. W. Schumacher, Phys. Rev. Lett. **64**, 1883–1886 (1990).
[4] H. Sakai, C. P. Safvan, J. J. Larsen, K. M. Hilligsoe, K. Hald, and H. Stapelfeldt, J. Chem. Phys. **110**, 10235–10238 (1999).
[5] M. Lein, N. Hay, R. Velotta, J. P. Marangos, and P. L. Knight, Phys. Rev. A **66**, 023805(1–6) (2002).
[6] Y. Yu, J. Xu, Y. Fu, H. Xiong, H. Xu, J. Yao, B. Zeng, W. Chu, J. Chen, Y. Cheng, and Z. Xu, Phys. Rev. A **80**, 053423(1–6) (2009).
[7] Y. L. Zhang, Q. D. Chen, H. Xia, and H. B. Sun, Nano Today, **5**, 435–448 (2010).
[8] K. Sugioka and Y. Cheng, Light Sci. Appl. **3**, e149 (2014).
[9] X. Xie, K. Doblhoff-Dier, S. Roither, M. S. Schoffler, D. Kartashov, H. L. Xu, T. Rathje, G. G. Paulus, A. Baltuska, S. Grafe, and M. Kitzler, Phys. Rev. Lett. **109**, 243001(1–5) (2012).
[10] S. L. Chin, S. A. Hosseini, W. Liu, Q. Luo, F. Théberge, N. Aközbek, A. Becker, V. P. Kandidov, O. G. Kosareva, and H. Schroeder, Can. J. Phys. **83**, 863–905 (2005).
[11] A. Couairon and A. Mysyrowicz, Phys. Rep. **441**, 47–189 (2007).
[12] L. Berge, S. Skupin, R. Nuter, J. Kasparian, and J.-P. Wolf, Rep. Prog. Phys. **70**, 1633–1713 (2007).
[13] J. Kasparian and J. P. Wolf, Opt. Exp. **16**, 466–493 (2008).
[14] S. L. Chin, Femtosecond Laser Filamentation (Springer, New York, 2010).
[15] S. L. Chin, T. Wang, C. Marceau, J. Wu, J. S. Liu, O. Kosareva, N. Panov, Y. P. Chen, J. F. Daigle, S. Yuan, A. Azarm, W. Liu, T. Seideman, H. Zeng, M. Richardson, R. Li, and Z. Xu, Laser Phys. **22**, 1–53 (2012).
[16] J. Kasparian, R. Sauerbrey, and S.L. Chin, Appl. Phys. B **71**, 877–879 (2000).
[17] A. Becker, N. Aközbek, K. Vijayalakshmi, E. Oral, C. M. Bowden, and S. L. Chin, Appl. Phys. B **73**, 287–290 (2001).
[18] H. Zhang, C. Jing, J. Yao, G. Li, B. Zeng, W. Chu, J. Ni, H. Xie, H. L. Xu, S. L. Chin, K. Yamanouchi, Y. Cheng, and Z. Z. Xu, Phys. Rev. X **3**, 041009(1–6) (2013).
[19] H. L. Li, H. L. Xu, B. S. Yang, Q. D. Chen, T. Zhang, and H. B. Sun, Opt. Lett. **38**, 1250–1252 (2013).
[20] P. Bejot, J. Kasparian, S. Henin, V. Loriot, T. Vieillard, E. Hertz, B. Lavorel, and J. P. Wolf, Phys. Rev. Lett. **104**, 103903(1–4) (2010).
[21] C. Bree, A. Demircan, and G. Steinmeyer, Phys. Rev. Lett. **106**, 183902(1–4) (2011).
[22] N. A. Panov, V. A. Makarov, V. Y. Fedorov, and O. G. Kosareva, Opt. Lett. **38**, 537–539 (2013).
[23] C. D'Amico, A. Houard, M. Franco, B. Prade, A. Mysyrowicz, A. Couairon, and V. T. Tikhonchuk, Phys. Rev. Lett. **98**, 235002(1–4) (2007).
[24] Y. Liu, A. Houard, B. Prade, S. Akturk, A. Mysyrowicz, and V. T. Tikhonchuk, Phys. Rev. Lett. **99**, 135002(1–4) (2007).
[25] J. L. Liu, J. M. Dai, S. L. Chin, and X. C. Zhang, Nature Photon. **4**, 627–631 (2010).
[26] J. F. Daigle, F. Théberge, M. Henriksson, T. J. Wang, S. Yuan, M. Châteauneuf, J. Dubois, M. Piché, and S. L. Chin, Opt. Exp. **20**, 6825–6834 (2012).
[27] Y. Bai, L. Song, R. Xu, C. Li, P. Liu, Z. Zeng, Z. Zhang, H. Lu, R. Li, and Z. Xu, Phys. Rev. Lett. **108**, 255004(1–5) (2012).
[28] B. Forestier, A. Houard, I. Revel, M. Durand, Y. B. Andre, B. Prade, A. Jarnac, J. Carbonnel, M. LeNeve, J. C. deMiscault, B. Esmiller, D. Chapuis, and A. Mysyrowicz, AIP Adv. **2**, 012151(1–13) (2012).
[29] P. Rohwetter, J. Kasparian, K. Stelmaszczyk, Z. Q. Hao, S. henin, N. Lascoux, W. M. Nakaema, Y. Petit, M. Queisser, R. Salame, E. Salmon, L. Woster, and J. P. Wolf, Nature Photon. **4**, 451–456 (2010).
[30] J. Ju, J. Liu, C. Wang, H. Sun, W. Wang, X. Ge, C. Li, S.L. Chin, R. Li, and Z. Xu, Opt. Lett. **37**, 1214–1216 (2012).
[31] J. Ju, H. Y. Sun, A. Sridharan, T.-J. Wang, C. Wang, J. Liu, R. Li, Z. Xu, and S. L. Chin, Phys. Rev. E **88**, 062803(1–7) (2013).

[32] H. Sun, J. Liu, C. Wang, J. Ju, Z. Wang, W. Wang, X. Ge, C. Li, S. L. Chin, R. Li, and Z. Xu, Opt. Exp. **21**, 9255–9266 (2013).
[33] Q. Luo, W. Liu, and S. L. Chin, Appl. Phys. B **76**, 337–340 (2003).
[34] J. P. Yao, B. Zeng, H. L. Xu, G. Li, W. Chu, J. Ni, H. Zhang, S. L. Chin, Y. Cheng, and Z. Z. Xu, Phys. Rev. A **84**, 051802(1–5) (2011).
[35] T. Wang, J. Ju, J. Daigle, S. Yuan, R. Li, and S. L. Chin, Laser. Phys. Lett. **10**, 125401(1–6) (2013).
[36] W. Chu, G. Li, H. Xie, J. Ni, J. Yao, B. Zeng, H Zhang, C. Jing, H. L. Xu, Y. Cheng, and Z. Z. Xu, Laser Phys. Lett. **11**, 015301(1–6) (2014).
[37] G. Point, Y. Liu, Y. Brelet, S. Mitryukovskiy, P. J. Ding, A. Houard, and A. Mysyrowicz, Opt. Lett. **39**, 1725–1728 (2014).
[38] C. P. Hauri, W. Kornelis, F. W. Helbing, A. Heinrich, A. Couairon, A. Mysyrowicz, J. Biegert, and U. Keller, Appl. Phys. B **79**, 673–677 (2004).
[39] S. Akturk, C. L. Arnold, B. Zhou, and A. Mysyrowicz, Opt. Lett. **34**, 1462–1464 (2009).
[40] N. Aközbek, A. Iwasaki, A. Becker, M. Scalora, S. L. Chin, and C. M. Bowden, Phys. Rev. Lett. **89**, 143901(1–4) (2002).
[41] T. Popmintchev, M. C. Chen, D. Popmintchev, P. Arpin, S. Brown, S. Ališauskas, G. Andriukaitis, T. Balciunas, O. D. Mucke, A. Pugzlys, A. Baltuška, B. Shim, S. E. Schrauth, G. Gaeta, C. Hernandez-Garcia, L. Plaja, A. Becker, A. Jaron-Becker, M. M. Murnane, and H. C. Kapteyn, Science **336**, 1287–1291 (2012).
[42] H. Zhou, W. X. Li, L. P. Shi, D. Wang, L. G. Ding, and H. P. Zeng, Laser Phys. Lett. **11**, 025402(1–4) (2014).
[43] A. Talebpour, M. Abdel-Fattah, A. D. Bandrauk, and S. L. Chin, Laser Phys. **11**, 68–76 (2001).
[44] H. L. Xu, Y. Kamali, C. Marceau, P. T. Simard, W. Liu, J. Bernhardt, G. Méjean, P. Mathieu, G. Roy, J.-R Simard, and S. L. Chin, Appl. Phys. Lett. **90**, 101106(1–3) (2007).
[45] J. Yao, G. Li, X. Jia, X. Hao, B. Zeng, C. Jing, W. Chu, J. Ni, H. Zhang, H. Xie, C. Zhang, Z. Zhao, J. Chen, X. Liu, Y. Cheng, and Z. Xu, Phys. Rev. Lett. **111**, 133001(1–5) (2013).
[46] J.-F. Gravel, Q. Luo, D. Boudreau, X. P. Tang, and S. L. Chin, Anal. Chem. **76**, 4799–4805 (2004).
[47] H. L. Xu and S. L. Chin, Sensors **11**, 32–53 (2011).
[48] S. L. Chin, H. L. Xu, Q. Luo, F. Théberge, W. Liu, J. F. Daigle, Y. Kamali, P. T. Simard, J. Bernhardt, S. A. Hosseini, M. Sharifi, G. Méjean, A. Azarm, C. Marceau, O. Kosareva, V. P. Kandidov, N. Aközbek, A. Becker, G. Roy, P. Mathieu, J. R. Simard, M. Châteauneuf, and J. Dubois, Appl. Phys. B **95**, 1–12 (2009).
[49] J. Kasparian, M. Rodriguex, G Méjean, J. Yu, E. Salmon, H. Wille, R. Bourayou, S. Frey, Y.-B. André, A. Mysyrowicz, R. Sauerbrey, J.-P. Wolf, and L. Wöste, Science **301**, 61–64 (2001).
[50] S. L. Chin, A. Talebpour, J. Yang, S. Petit, V. P. Kandidov, O. G. Kosareva, and M. P. Tamarov, Appl. Phys. B **74**, 67–76 (2002).
[51] M. Rodriguez, R. Bourayou, G. Méjean, J. Kasparian, J. Yu, E. Salmon, A. Scholz, B. Stecklum, J. Eislöffel, U. Laux, P. Hatzes, R. Sauerbrey, L. Wöste, and J. P. Wolf, Phys. Rev. E **69**, 036607(1–7) (2004).
[52] G. Méchain, G. Méjean, R. Ackermann, P. Rohwetter, Y. B. André, J. Kasparian, B. Prade, K. Stelmaszczyk, J. Yu, E. Salmon, W. Winn, L. A. Schlie, A. Mysyrowicz, R. Sauerbrey, L. Wöste, and J.-P. Wolf, Appl. Phys. B **80**, 785–789 (2005).
[53] R. Ackermann, G. Méjean, J. Kasparian, J. Yu, E. Salmon, and J.-P. Wolf, Opt. Lett. **31**, 86–88 (2006).
[54] S. Hosseini, A. Azarm, J.-F. Daigle, Y. Kamali, and S. L. Chin, Opt. Commun. **316**, 61–66 (2014).
[55] W. Chu, H. L. Li, J. Ni, B. Zeng, J. Yao, H. Zhang, G. Li, C. Jing, H. Xie, H. L. Xu, K. Yamanouchi, and Y. Cheng, Appl. Phys. Lett. **104**, 091106(1–3) (2014).
[56] S. Svanberg, Differential absorption Lidar (DIAL), in Air monitoring by spectroscopic techniques, M. W. Sigrist (ed.), (Wiley, New York, 1994) pp. 85–162.
[57] H. I. Schiff, G. I. Mackay, and J. Bechara, The Use of Tunable Diode Laser Absorption Spectroscopy for Atmospheric Measurements, In Air Monitoring by Spectroscopic Techniques, M. W. Sigrist (ed.), (Wiley, New York 1994) pp. 239–335.
[58] R. M. Measures, Laser remote sensing: Fundamentals and Applications (Wiley, New York, 1984).
[59] A. Azarm, H. L. Xu, Y. Kamali, J. Bernhardt, D. Song, A. Xia, Y. Teranishi, S. H. Lin, F. Kong, and S. L. Chin, J. Phys. B **41**, 225601(1–4) (2008).
[60] F. Kong, Q. Luo, H. L. Xu, M. Sharifi, D. Song, and S. L. Chin, J. Chem. Phys. **125**, 133320(1–5) (2006).
[61] F. Kong and S. L. Chin, Non-Coulomb Explosions of Molecules in Intense Laser Fields, in Progress in Ultrafast Intense Laser Science III, K. Yamanouchi, S. L. Chin, P. Agostini, and G. Ferrante (eds.), (Springer-Verlag, Berlin, 2008) pp.113–127.
[62] H. Hasegawa, A. Hishikawa, and K. Yamanouchi, Chem. Phys. Lett. **349**, 57–63 (2001).
[63] H. L. Xu, A. Azarm, J. Bernhardt, Y. Kamali, and S. L. Chin, Chem. Phys. **360**, 171–175 (2009).
[64] H. R. Lange, A. Chiron, J.-F. Ripoche, A. Mysyrowicz, P. Breger, and P. Agostini, Phys. Rev. Lett. **81**, 1611–1613 (1998).
[65] J. Bernhardt, P. T. Simard, W. Liu, H.L. Xu, F. Théberge, A. Azarm, J. F. Daigle, and S. L. Chin, Opt. Commun. **281**, 2248–2251 (2008).
[66] S. Xu, J. Bernhardt, M. Sharifi, W. Liu, and S. L. Chin, Laser Phys. **22**, 195–202 (2012).
[67] F. Théberge, W. Liu, P. T. Simard, A. Becker, and S. L. Chin, Phys. Rev. E **74**, 036406(1–7) (2006).
[68] J.-F. Daigle, A. Jaron-Becker, S. Hosseini, T.-J. Wang, Y. Kamali, G. Roy, A. Becker, and S. L. Chin, Phys. Rev. A **82**, 023405(1–5) (2010).
[69] J. Bernhardt, W. Liu, F. Théberge, H.L. Xu, J. F. Daigle, M. Chateauneuf, J. Dubois, and S. L. Chin, Opt. Commun. **281**, 1268–1274 (2008).
[70] G. Rodriguez, A. R. Valenzuela, B. Yellampalle, M. J. Schmitt, and K. Y. Kim, J. Opt. Soc. Am. B **25**, 1988–1997 (2008).
[71] D. Abdollahpour, S. Suntsov, D. G. Papazoglou, and S. Tzortzakis, Opt. Exp. **19**, 16866–16871 (2011).

[72] V. P. Kandidov, O. G. Kosareva, I. S. Golubtsov, W. Liu, A. Becker, N. Akozbek, C. M. Bowden, and S. L. Chin, Appl. Phys. B **77**, 149–165 (2003).
[73] W. Liu and S. L. Chin, Opt. Exp. **13**, 5750–5755 (2005).
[74] W. Liu, Q. Luo, F. Théberge, H. L. Xu, S. A. Hosseini, S. M. Sarifi, and S. L. Chin, Appl. Phys. B **82**, 373–376 (2006).
[75] M. Durand, A. Houard, B. Prade, A. Mysyrowicz, A. Durécu, B. Moreau, D. Fleury, O. Vasseur, H. Borchert, K. Diener, R. Schmitt, F. Théberge, M. Chateauneuf, J.-F. Daigle, and J. Bubois, Opt. Exp. **21**, 26836–26845 (2013).
[76] F. Vidal and T. W. Johnston, Phys. Rev. Lett. **77**, 1282–1285 (1996).
[77] M. Mlejnek, M. Kolesik, J. V. Moloney, and E. M. Wright, Phys. Rev. Lett. **83**, 2938–2941 (1999).
[78] S. A. Hosseini, Q. Luo, B. Ferland, W. Liu, S. L. Chin, O. G. Kosareva, N. A. Panov, N. Aközbek, and V. P. Kandidov, Phys. Rev. A **70**, 033802(1–12) (2004).
[79] G. Méchain, A. Couairon, M. Franco, B. Prade, and A. Mysyrowicz, Phys. Rev. Lett. **93**, 035003(1–4) (2004).
[80] W. Liu, F. Theberge, J. F. Daigle, P. T. Simard, S. M. Sarifi, Y. Kamali, H. L. Xu, and S. L. Chin, Appl. Phys. B **85**, 55–58 (2006).
[81] G. Fibich, Y. Sivan, Y. Ehrlich, E. Louzon, M. Fraenkel, S. Eisenmann, Y. Katzir, and A. Zigler, Opt. Exp. **14**, 4946–4957 (2006).
[82] T. Pfeifer, L. Gallmann, M. J. Abel, D.M. Neumark, and S. R. Leone, Opt. Lett. **31**, 2326–2328 (2006).
[83] Y. Fu, H. Xiong, H. Xu, J. Yao, B. Zeng, W. Chu, Y. Cheng, Z. Xu, W. Liu, and S. L. Chin, Opt. Lett. **34**, 3752–3754 (2009).
[84] Z. Hao, J. Zhang, T. Xi, X. Yuan, Z. Zheng, X. Lu, M. Yu, Y. Li, Z. Wang, W. Zhao, and Z. Wei, Opt. Exp. **15**, 16102–16109 (2007).
[85] J. F. Daigle, O. Kosareva, N. Panov, M. Bégin, F. Lessard, C. Marceau, Y. Kamali, G. Roy, V. P. Kandidov, and S. L. Chin, Appl. Phys. B **94**, 249–257 (2009).
[86] Q. Luo, J. Yu, S. A. Hosseini, W. Liu, B. Ferland, G. Roy, and S. L. Chin, Appl. Opt. **44**, 391–397 (2005).
[87] Y. Kamali, Q. Sun, J.-F. Daigle, A. Azarm, J. Bernhardt, and S. L. Chin, Opt. Commun. **281**, 950–954 (2009).
[88] Q. Luo, S. A. Hosseini, W. Liu, J. F. Gravel, O. G. Kosareva, N. A. Panov, N. Aközbek, V. P. Kandidov, G. Roy, and S. L. Chin, Appl. Phys. B **80**, 35–38 (2005).
[89] J. F. Daigle, Y. Kamali, J. Bernhardt, W. Liu, C. Marceau, A. Azarm, and S. L. Chin, Opt. Commun. **281**, 3327–3335 (2008).
[90] J. Wu, H. Cai, Y. Peng, Y. Tong, A. Couairon, and H. P. Zeng, Laser Phys. **19**, 1759–1768 (2009).
[91] M. Bellec, P. Panagiotopoulos, D. G. Papazoglou, N. K. Efremidis, A. Couairon, and S. Tzortzakis, Phys. Rev. Lett. **109**, 113905 (2012).
[92] N. Jhajj, E. W. Rosenthal, R. Birnbaum, J. K. Wahlstrand, and H. M. Milchberg, Phys. Rev. X **4**, 011027 (2014).
[93] P. Panagiotopoulos, D. G. Papazoglou, A. Couairon, and S. Tzortzakis, Nature Commun. **4**, 2622 (2013).
[94] R. Ackermann, E. Salmon, N. Lascoux, J. Kasparian, P. Rohwetter, K. Stelmaszczyk, S. Li, A. Lindinger, L. Wöste, P. Béjot, L. Bonacina, and J.-P. Wolf, Appl. Phys. Lett. **89**, 171117 (2006).
[95] M. Mlejnek, E. M. Wright, and J. V. Moloney, Opt. Lett. **23**, 382–384 (1998).
[96] O. G. Kosareva, N. A. Panov, N. Aközbek, V. P. Kandidov, Q. Luo, S. A. Hosseini, W. Liu, J. F. Gravel, G. Roy, and S. L. Chin, Appl. Phys. B **82**, 111–122 (2006).
[97] F. Courvoisier, V. Boutou, J. Kasparian, E. Salmon, G. Méjean, J. Yu, and J. P. Wolf, Appl. Phys. Lett. **83**, 213–215 (2003).
[98] A. Dubietis, E. Kucinskas, G. Tamosauskas, E. Gaizauskas, M. A. Porras, and P. Di Trapani, Opt. Lett. **29**, 2893–2895 (2004).
[99] M. Kolesik and J. V. Moloney, Opt. Lett. **29**, 590–592 (2004).
[100] O. G. Kosareva, V. P. Kandidov, A. Brodeur, C. Y. Chien, and S. L. Chin, Opt. Lett. **22**, 1332–1334 (1997).
[101] S. Eisenmann, J. Penano, P. Sprangle, and A. Zigler, Phys. Rev. Lett. **100**, 155003(1–4) (2008).
[102] W. Liu, F. Théberge, E. Arévalo, J. F. Gravel, A. Becker, and S. L. Chin, Opt. Lett. **30**, 2602–2604 (2005).
[103] W. Liu, J. F. Gravel, F. Théberge, A. Becker, and S. L. Chin, Appl. Phys. B **80**, 857–860 (2005).
[104] H. L. Xu, T. Okino, K. Nakai, and K. Yamanouchi, Ultrafast Hydrogen Migration in Hydrocarbon Molecules Driven by Intense Laser Fields, in Progress in Ultrafast Intense Laser Science VII, K. Yamanouchi, D. Charalambidis, and D. Normand (eds.) (Springer-Verlag, New York, 2011) pp. 35–52.
[105] H. L. Xu, J. Bernhardt, P. Mathieu, G. Roy, and S. L. Chin, J. Appl. Phys. **101**, 033124(1–6) (2007).
[106] Q. Luo, S. A. Hosseini, B. Ferland, and S. L. Chin, Opt. Commun. **233**, 411–416 (2004).
[107] A. Iwasaki, N. Aközbek, B. Ferland, Q. Luo, G. Roy, C. M. Bowden, and S. L. Chin, Appl. Phys. B **76**, 231–236 (2003).
[108] S. A. Hosseini, J. Yu, Q. Luo, and S. L. Chin, Appl. Phys. B **79**, 519–523 (2004).
[109] H. L. Xu, J. F. Daigle, Q. Luo, and S. L. Chin, Appl. Phys. B **82**, 655–658 (2006).
[110] Q. Luo, H. L. Xu, S. A. Hosseini, J. F. Daigle, F. Théberge, M. Sharifi, and S. L. Chin, Appl. Phys. B **82**, 105–109 (2006).
[111] J. F. Daigle, Y. Kamali, M. Châteauneuf, G. Tremblay, F. Théberge, J. Dubois, G. Roy, and S. L. Chin, Appl. Phys. B **97**, 701–713 (2009).
[112] J. F. Daigle, Y. Kamali, G. Roy, and S. L. Chin, Appl. Phys. B **93**, 759–762 (2008).
[113] T. Fujii, N. Goto, M. Miki, T. Nayuki, and K. Nemoto, Opt. Lett. **31**, 3456–3458 (2006).
[114] J. F. Daigle, G. Méjean,W. Liu, F. Théberge, H. L. Xu, Y. Kamali, J. Bernhardt, A. Azarm, Q. Sun, P. Mathieu, G. Roy, J. R. Simard, and S. L. Chin, Appl. Phys. B **87**, 749–754 (2007).
[115] J. F. Daigle, P. Mathieu, G. Roy, J. R. Simard, and S. L. Chin, Opt. Commun. **278**, 147–152 (2007).
[116] G. Méjean, J. Kasparian, J. Yu, S. Frey, E. Salmon, and J. P. Wolf, Appl. Phys. B **78**, 535–537 (2004).
[117] A. Becker, A. D. Bandrauk, and S. L. Chin, Chem. Phys. Lett. **343**, 345–350 (2001).
[118] S. Mitryukovskiy, Y. Liu, P. Ding, A. Houard, and A. Mysyrowicz, Opt. Exp. **22**, 12750–12759 (2014).

[119] D. Kartashov, S. Ališauskas, A. Baltuška, A. Schmitt-Sody, W. Roach, and P. Polynkin, Phys. Rev. A **88**, 041805(1–4) (2013).
[120] D. Song, A. Azarm, Y. Kamali, K. Liu, A. Xia, Y. Teranishi, S. Lin, F. Kong, and S. L. Chin, J. Phys. Chem. A **114**, 3087–3095 (2010).
[121] H. L. Xu, A. Azarm, and S. L. Chin, Appl. Phys. Lett. **98**, 141111(1–3) (2011).
[122] M. Sharifi, F. Kong, S. L. Chin, H. Mineo, Y. Dyakov, A. M. Mebel, S. D. Chao, M. Hayashi, and S. H. Lin, J. Phys. Chem. A **111**, 9405–9416 (2007).
[123] C. Cornaggia and P. Hering, Phys. Rev. A **62**, 023403(1–13) (2000).
[124] H. Xu, T. Okino, and K. Yamanouchi, Chem. Phys. Lett. **469**, 255–260 (2009).
[125] J. H. Posthumus, Rep. Prog. Phys. **67**, 623–665 (2004).
[126] V. V. Lozovoy, X. Zhu, T. C. Gunaratne, D. Ahmasi Harris, J. C. Shane, and M. Dantus, J. Phys. Chem. A **112**, 3789–3812 (2008).
[127] B. S. Yang, L. Zhang, H. L. Xu, R. X. Li, and K. Yamanouchi, Chin. J. Phys. **52**, 652–674 (2014).
[128] J. Ullrich, R. Moshammer, A. Dorn, R. Dörner, L. Ph. H. Schmidt, and H. Schmidt- Böcking, Rep. Prog. Phys. **66**, 1463–1545 (2003).
[129] R. Dörner, V. Mergel, O. Jagutzki, L. Spielberger, J. Ullrich, R. Moshammer, and H. Schmidt-Böcking, Phys. Rep. **330**, 95–192 (2000).
[130] H. L. Xu, T. Okino, and K. Yamanouchi, J. Chem. Phys. **131**, 151102(1–4) (2009).
[131] R. Itakura, K. Yamanouchi, T. Tanabe, T. Okamoto, and F. Kannari, J. Chem. Phys. **119**, 4179–4186 (2003).
[132] H. Yazawa, T. Shioyama, H. Hashimoto, F. Kannari, R. Itakura, and K. Yamanouchi, Appl. Phys. B **98**, 275–282 (2010).
[133] L. Zhang, S. Roither, X. Xie, D. Kartashov, M. Schöffler, H. L. Xu, A. Iwasaki, S. Gräfe, T. Okino, K. Yamanouchi, A. Baltuška, and M. Kitzler, J. Phys. B **45**, 085603(1–12) (2012).
[134] H. L. Xu, T. Okino,T. Kudou, K. Yamanouchi, S. Roither, M. Kitzler, A. Baltuska, and S. L. Chin, J. Phys. Chem. A **116**, 2686–2690 (2012).
[135] T.-J. Wang, H. L. Xu, J.-F. Daigle, A. Sridharan, S. Yuan, and S. L. Chin, Opt. Lett. **37**, 1706–1708 (2012).
[136] S. Yuan, T. J. Wang, P. Lu, S. L. Chin, and H. P. Zeng, Appl. Phys. Lett. **104**, 091113(1–4) (2014).
[137] Y. Petit, S. Henin, J. Kasparian, and J. P. Wolf, Appl. Phys. Lett. **97**, 021108(1–3) (2010).
[138] T. Leisner, D. Duft, O. Mohler, H. Saathoff, M. Schnaiter, S. Henin, K. Stelmaszczyk, M. Petrarca, R. Delagrange, Z. Q. Hao, J. Luder, Y. Petit, P. Rohwetter, J. Kasparian, J. P. Wolf, and L. Woste, Proc. Natl. Acad. Sci. USA **110**, 10106–10110 (2013).
[139] S. Mahesh and D. P. Mishra, Fuel **89**, 2145–2148 (2010).
[140] H. L. Li, X. Y. Wei, H.L. Xu, S. L. Chin, K. Yamanouchi, H. B. Sun, Sens. Actuators B **203**, 887–890 (2014).
[141] D. Kartashov, S. Ališauskas, G. Andiukaitis, A. Pugžlys, M. Shneider, A. Zheltikov, S. L. Chin, and A. Baltuška, Phys. Rev. A **86**, 033831(1–8) (2012).
[142] J. Yao, G. Li, C. Jing, B. Zeng, W. Chu, J. Ni, H. Zhang, H. Xie, C. Zhang, H. Li, H. Xu, S. L. Chin, Y. Cheng, and Z. Xu, New J. Phys. **15**, 023046(1–10) (2013).
[143] J. Ni, W. Chu, C. Jing, H. Zhang, B. Zeng, J. Yao, G. Li, H. Xie, C. Zhang, H. Xu, S. L. Chin, Y. Cheng, and Z. Xu, Opt. Exp. **21**, 8746–8752 (2013).
[144] Y. Liu, Y. Brelet, G. Point, A. Houard, and A. Mysyrowicz, Opt. Exp. **21**, 22791–22798 (2013).
[145] C. Jing, H. Zhang, W. Chu, H. Xie, J. Ni, B. Zeng, G. Li, J. Yao, H. Xu, Y. Cheng, and Z. Xu, Opt. Exp. **22**, 3151–3156 (2014).
[146] B. Zeng, W. Chu, G. Li, J. Yao, H. Zhang, J. Ni, C. Jing, H. Xie, and Y. Cheng, Phys. Rev. A **89**, 042508(1–5) (2014).
[147] W. Chu, B. Zeng, J. P. Yao, H. L. Xu, J. Ni, G. Li, H. Zhang, F. He, C. Jing, Y. Cheng, and Z. Z. Xu, Europhys. Lett. **97**, 64004(1–5) (2012).
[148] S. Yuan, T. Wang, Y. Teranishi, A. Sridharan, S. H. Lin, H. Zeng, and S. L. Chin, Appl. Phys. Lett. **102**, 224102(1–5) (2013).
[149] A. Dogariu, J. B. Michael, M. O. Scully, and R. B. Miles, Science **331**, 442–445 (2011).
[150] P. R. Hemmer, P. Polynkin, T. Siebert, A. V. Sokolov, P. Sprangle, and M. O. Scully, Proc. Natl. Acad. Sci. USA **108**, 3130–3134 (2011).
[151] P. Sprangle, J. Peñano, B. Hafizi, D. Gordon, and M. Scully, Appl. Phys. Lett. **98**, 211102(1–3) (2011).
[152] M. N. Shneider, A. Baltuška, and A. M. Zheltikov, J. Appl. Phys. **110**, 083112(1–7) (2011).
[153] J. Peñano, P. Sprangle, B. Hafizi, D. Gordon, and R. Fernsler, J. Appl. Phys. **111**, 033105(1–8) (2012).
[154] S. L. Chin, H. L. Xu, Y. Cheng, Z. Z. Xu, and K. Yamanouchi, Chin. Opt. Lett. **11**, 013201(1–3) (2013).
[155] H. Zhang, C. Jing, G. Li, H. Xie, J. Yao, B. Zeng, W. Chu, J. Ni, H. L. Xu, and Y. Cheng, Phys. Rev. A **88**, 063417(1–5) (2013).
[156] G. Li, C. Jing, B. Zeng, H. Xie, J. Yao, W. Chu, J. Ni, H. Zhang, H. L. Xu, Y. Cheng, and Z. Z. Xu, Phys. Rev. A **89**, 033833(1–5) (2014).
[157] T. Wang, J. F. Daigle, J. Ju, S. Yuan, R. Li, and S. L. Chin, Phys. Rev. A **88**, 053429(1–5) (2013).
[158] J. Ni, W. Chu, H. Zhang, B. Zeng, J. Yao, G. Li, C. Jing, H. Xie, H. Xu, Y. Cheng, and Z. Xu, Opt. Lett. **39**, 2250–2253 (2014).